

Magnetothermal properties of the Heisenberg-Ising orthogonal-dimer chain with triangular XXZ clusters

Vadim Ohanyan¹ and Andreas Honecker^{2,3}

¹*Department of Theoretical Physics, Yerevan State University, Al. Manoogian 1, 0025, Yerevan, Armenia**

²*Institut für Theoretische Physik, Georg-August-Universität Göttingen, 37077 Göttingen, Germany*

³*Fakultät für Mathematik und Informatik, Georg-August-Universität Göttingen, 37073 Göttingen, Germany*

(Dated: March 21, 2012; revised July 22, 2012)

We study a spin-1/2 model with triangular XXZ -clusters on the orthogonal-dimer chain in the presence of an external magnetic field. First, we discuss the case where the triangular clusters are coupled via intermediate “classical” Ising spins. Diagonalization of the triangular XXZ -clusters yields the exact ground states; finite-temperature properties are computed exactly by an additional transfer-matrix step. A detailed analysis reveals a large variety of ground states at magnetization M equal to fractions 0, 1/4, and 1/2 of the saturation magnetization $M = 1$. Some of these ground states break translational symmetry spontaneously and give rise to doubling of the unit cell. In a second part we present complementary numerical data for the spin-1/2 Heisenberg model on the orthogonal-dimer chain. We analyze several examples of $T = 0$ magnetization curves, entropy as a function of temperature T and magnetic field, and the associated magnetic cooling rate. Comparison of the two models shows that in certain situations the simplified exactly solvable model yields a qualitatively or sometimes even quantitatively accurate description of the more challenging quantum model, including a case which may be relevant to experimental observations of an enhanced magnetocaloric effect in the two-dimensional compound $\text{SrCu}_2(\text{BO}_3)_2$.

PACS numbers: 75.10.Pq; 75.30.Kz; 75.40.Cx; 75.40.Mg

I. INTRODUCTION

There is a two-fold interest in the statistical mechanics of many-body lattice spin systems. On the one hand, one-dimensional integrable many-body models^{1,2} have been intensively investigated, if not since the seminal 1931 paper of Hans Bethe,³ then at least since the 1960-s. A linear chain of localized spins which interact with each other via exchange interactions (Heisenberg chain) is the key component of almost all such models. The research on integrable spin chains is often considered to be separated from the underlying physical context, as their integrability is deeply related to modern algebraic structures (see for instance Refs. 4 and 5) and attracts mainly mathematical physicists. On the other hand, various lattice spin systems serve as the basis for *physical models* for describing magnetism of materials and related phenomena. As a rule, quantum lattice spin models corresponding to real materials rarely admit exact solutions. Therefore, one often has to resort to numerical calculations in order to obtain reliable results for the thermodynamic properties of such strongly correlated magnetic materials. However, for one-dimensional integrable models, there are powerful mathematical tools allowing one, at least in principle, to compute the thermodynamic functions exactly.^{2,6} Despite their impressive efficiency, these methods are applicable only if the underlying lattice model is integrable, which is not always the case for real magnetic materials. However, there is another class of application for so-called classical one-dimensional lattice models, namely as effective descriptions of the conformations of macromolecules.⁷ In that case, one can obtain an analytical expression for the partition function and, thus,

for all thermodynamic functions.

Lattice spin models with quantum and classical spins,⁸ respectively Ising and Heisenberg^{9–19} or Hubbard interactions^{20,21} combine properties of both quantum and classical spin systems. They can be solved exactly by the classical transfer-matrix method, while the entries of the transfer matrix contain the contribution from the quantum clusters of the model. Such exact results obtained in one-dimensional models containing both quantum and classical interactions can shed light on the properties of the corresponding purely quantum ones and as a result into the more profound understanding of the thermodynamic behavior of magnetic materials with a one-dimensional arrangement of exchange bonds.^{8–21} For instance, certain qualitative properties of one-dimensional quantum spin systems can remain intact under the replacement of some or even all quantum exchange interactions by Ising ones. In particular, if the magnetization curve has an intermediate plateau at some fixed value of the magnetization, the same feature may persist also in the modified system, although the region of parameters at which it appears can be different.^{9,11} In some cases, one even finds a rather good quantitative correspondence between the exact magnetization curves obtained for the modified system and that obtained by numerical methods for the underlying fully quantum system.¹¹

Some real compounds may in fact be well approximated by such mixed Heisenberg-Ising models. One example is given by a family of trimetallic coordination polymer compounds.^{22–24} Due to the presence of highly anisotropic Dy^{3+} ions, these compounds yield a direct realization of low-dimensional spin systems with Ising and Heisenberg bonds. The single-chain magnet reported in

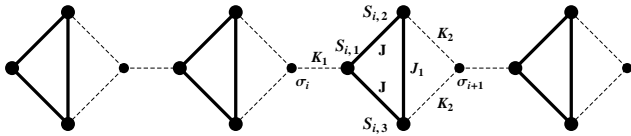


FIG. 1. “Orthogonal-dimer” chain constructed from triangles of quantum $s = 1/2$ spins (large circles) interacting with each other via Heisenberg XXZ interactions (thick solid lines) and assembled to a chain by “classical” Ising spins (small circles). One coupling constant (J_1) connects the quantum spins along a vertical line while a generally different coupling constant (J) connects the other two bonds in the quantum triangle. Further coupling constants are assigned to the Ising bonds connecting left (K_1) and right (K_2) spins with the corresponding “classical” spins σ_i and σ_{i+1} .

Ref. 22 is an example of a Heisenberg-Ising chain of triangles with three-spin linear quantum clusters; another interesting molecular magnet (spin ring) based on the highly anisotropic properties of the Dy^{3+} ions has been reported in Ref. 23. Both systems have been analyzed by the transfer-matrix solution of Heisenberg-Ising spin chains in Ref. 24. Another class of examples is given by chain magnets with two alternating magnetic ions, thus giving rise to alternating quantum and classical spins (see, e.g., Refs. 25–27).

Here we continue to apply the exact transfer-matrix calculation for elucidating the thermodynamic and ground-state magnetic properties of one-dimensional spin systems with Ising and Heisenberg bonds^{15–19,24} and perform an analysis of the similarities and discrepancies between magneto-thermal properties of the exactly solvable Heisenberg-Ising model and the underlying purely quantum Heisenberg system. We consider a one-dimensional $s = 1/2$ chain consisting of triangular clusters with XXZ Heisenberg interactions and single classical sites between them (see Fig. 1). Each spin at the single site is connected by bonds of Ising type with the two spins of its left triangle and with one spin of the right triangle. The corresponding arrangement of sites into a chain is known as “orthogonal-dimer” chain.^{28–31} However, since the symmetry of the chain is already reduced by the nature of the interactions, here we also allow for more general interactions.

The magnetization curve of the antiferromagnetic quantum orthogonal-dimer chain is famous for an infinite series of magnetization plateaux.³⁰ This infinite sequence of plateaux is caused by the local conservation of the total spin on each vertical dimer: for each k , a ground state of the infinite system can be constructed by a periodic sequence of k vertical dimers in the triplet state $s = 1$ with two singlet dimers at the end. In the Heisenberg-Ising case considered here, only the main plateaux with magnetization equal to 0, 1/4, and 1/2 of the quantum orthogonal-dimer chain are observed in the zero-temperature magnetization curve. Depending on parameters of the models, we find various ground states

with 4 and 8 sites per unit cell realized at these magnetization values. Some of these ground states give rise to a doubling of the unit cell and a corresponding spatial modulation of the local magnetization. The appearance of such structures may be attributed to the left-right asymmetry for the triangular quantum clusters. Similar observations were previously reported in Refs. 16 and 17 for the sawtooth chain with Ising and Heisenberg bonds.

This paper is organized as follows. In section II we present the model and describe the exact computation of thermodynamic properties using a classical transfer matrix. In section III we then specialize to zero temperature and describe the ground states. Section IV contains a discussion of the ground-state phase diagram in the presence of an external magnetic field. Section V presents some exact magnetization curves of the Heisenberg-Ising model for finite temperatures. Finally, in section VI, we present numerical results for the full quantum Heisenberg model and compare it to the Heisenberg-Ising system. In this comparison, we focus on two properties: the ground-state magnetization curve and the magnetocaloric effect. The paper ends with a conclusion.

II. THE MODEL AND ITS EXACT SOLUTION

We consider a spin chain consisting of $s = 1/2$ XXZ -Heisenberg triangular spin clusters, connected to each other via single spins situated between the triangles in such a way that each left-hand single spin is connected with the Ising bond σ_i - S_i^z to the single spin of a triangular cluster and each right-hand single spin is connected by the Ising bond to two spins in the vertical line of the triangular cluster (see Fig. 1). This chain is topologically equivalent to the famous orthogonal-dimer chain,^{28–31} albeit with more general interactions. The Hamiltonian of the system is conveniently represented as a sum of the single-block Hamiltonians \mathcal{H}_i

$$\mathcal{H} = \sum_{i=1}^L \left(\mathcal{H}_i - \frac{H_1}{2} (\sigma_i + \sigma_{i+1}) \right), \quad (1)$$

where

$$\begin{aligned} \mathcal{H}_i = J \{ & \Delta [S_{i,1}^x (S_{i,2}^x + S_{i,3}^x) + S_{i,1}^y (S_{i,2}^y + S_{i,3}^y)] \\ & + S_{i,1}^z (S_{i,2}^z + S_{i,3}^z) \} \\ & + J_1 (\Delta_1 (S_{i,2}^x S_{i,3}^x + S_{i,2}^y S_{i,3}^y) + S_{i,2}^z S_{i,3}^z) \\ & + K_1 \sigma_i^z S_{i,1}^z + K_2 \sigma_{i+1}^z (S_{i,2}^z + S_{i,3}^z) \\ & - H_2 (S_{i,1}^z + S_{i,2}^z + S_{i,3}^z). \end{aligned} \quad (2)$$

Here L is the number of blocks (cells) in the chain (the number of spins N is $4L$), $S_{i,a}$ stands for the spin operators of the i -th triangle in the chain, $a = 1, 2, 3$ numbers the three sites of the triangle, and σ_i^z is the z -component of the single spin situated at the left-hand side of the i -th triangle. Here, we allow the exchange interaction constants between the spins on the vertical line J_1 , Δ_1

and between the single spin of a triangle and spins on the vertical line J , Δ to be different as well as the interaction constants for left and right single spins, K_1 and K_2 , respectively. Magnetic fields acting on S -spins and σ -spins are also considered to be different.

We are going to derive exact expressions for all thermodynamic functions of the chain. To this end one should calculate the partition function

$$\mathcal{Z} = \sum_{(\sigma)} \text{Tr} \mathbf{S} e^{-\beta \sum_{i=1}^L (\mathcal{H}_i - \frac{H_1}{2} (\sigma_i + \sigma_{i+1}))}. \quad (3)$$

Spin variables of single spins can be regarded as classical Ising ones, as they contribute only their diagonal z -component and hence can be replaced with their eigenvalues $\pm 1/2$. Thus, in the partition function one should sum over all values of the σ_i and take a trace over the states of all spin operators \mathbf{S} . Due to the special structure of interactions, the partition function can be evaluated exactly. To proceed, we first note that the Hamiltonians of different blocks commute

$$[\mathcal{H}_i, \mathcal{H}_j] = 0. \quad (4)$$

Thus, one can expand the exponential in Eq. (3) and get the following expression

$$\mathcal{Z} = \sum_{(\sigma)} \prod_{i=1}^L e^{\beta \frac{H_1}{2} (\sigma_i + \sigma_{i+1})} \text{Tr}_i e^{-\beta \mathcal{H}_i}, \quad (5)$$

where Tr_i implies the trace over all states of the i -th block of the chain. The trace can be easily calculated once the block Hamiltonian \mathcal{H}_i is diagonalized, which can be achieved analytically in our case. One finds the following eigenvalues

$$\begin{aligned} \lambda_{1,2}(\sigma_i, \sigma_{i+1}) &= \frac{1}{4} (J_1 + 2J) \\ &\quad \pm \frac{1}{2} (K_1 \sigma_i + 2K_2 \sigma_{i+1}) \mp \frac{3}{2} H_2, \\ \lambda_{3,4}(\sigma_i, \sigma_{i+1}) &= -\frac{1}{4} J_1 (1 + 2\Delta_1) \pm \frac{1}{2} K_1 \sigma_i \mp \frac{1}{2} H_2, \\ \lambda_{5,6}(\sigma_i, \sigma_{i+1}) &= \frac{1}{4} (J_1 \Delta_1 - J - Q_{\mp \sigma_i, \pm \sigma_{i+1}}) \\ &\quad \pm \frac{1}{2} K_2 \sigma_{i+1} \mp \frac{1}{2} H_2, \\ \lambda_{7,8}(\sigma_i, \sigma_{i+1}) &= \frac{1}{4} (J_1 \Delta_1 - J + Q_{\mp \sigma_i, \pm \sigma_{i+1}}) \\ &\quad \pm \frac{1}{2} K_2 \sigma_{i+1} \mp \frac{1}{2} H_2, \end{aligned} \quad (6)$$

where the following abbreviation is adopted:

$$Q_{\sigma, \sigma'} = \sqrt{8J^2 \Delta^2 + (J_1(1 - \Delta_1) - J + 2(K_1 \sigma + K_2 \sigma'))^2}. \quad (7)$$

The corresponding eigenstates carry a definite value of $S_{\text{tot}}^z = S_1^z + S_2^z + S_3^z$: the eigenvalues $\lambda_{1,2}$ correspond to states with $S_{\text{tot}}^z = \pm 3/2$ and the remaining eigenvalues to $S_{\text{tot}}^z = \pm 1/2$. The eigenvectors read:

$$\begin{aligned} \lambda_1: \quad |v_{\frac{3}{2}}\rangle &= |\uparrow\uparrow\uparrow\rangle, \\ \lambda_2: \quad |v_{-\frac{3}{2}}\rangle &= |\downarrow\downarrow\downarrow\rangle, \\ \lambda_3: \quad |v_{\frac{1}{2}, a}\rangle &= \frac{1}{\sqrt{2}} (|\uparrow\uparrow\downarrow\rangle - |\uparrow\downarrow\uparrow\rangle), \\ \lambda_4: \quad |v_{-\frac{1}{2}, a}\rangle &= \frac{1}{\sqrt{2}} (|\downarrow\downarrow\uparrow\rangle - |\downarrow\uparrow\downarrow\rangle), \\ \lambda_{5,7}: \quad |v_{\frac{1}{2}, s}^{\pm}\rangle &= \frac{1}{\sqrt{2 + c_{\pm}^2}} (|\uparrow\uparrow\downarrow\rangle + |\uparrow\downarrow\uparrow\rangle + c_{\pm} |\downarrow\uparrow\uparrow\rangle), \\ \lambda_{6,8}: \quad |v_{-\frac{1}{2}, s}^{\pm}\rangle &= \frac{1}{\sqrt{2 + \bar{c}_{\pm}^2}} (|\downarrow\downarrow\uparrow\rangle + |\downarrow\uparrow\downarrow\rangle + \bar{c}_{\pm} |\uparrow\downarrow\downarrow\rangle). \end{aligned} \quad (8)$$

In each state $|\dots\rangle$ the first, second, and third arrow denotes an z -eigenbasis of $\mathbf{S}_{i,1}$, $\mathbf{S}_{i,2}$, and $\mathbf{S}_{i,3}$, respectively. Furthermore, we have introduced the following abbreviations

$$\begin{aligned} c_{\pm} &= \frac{J_1(1 - \Delta_1) - J + 2(K_2 \sigma_R - K_1 \sigma_L) \pm Q_{-\sigma_L, \sigma_R}}{J\Delta}, \\ \bar{c}_{\pm} &= \frac{J_1(1 - \Delta_1) - J - 2(K_2 \sigma_R - K_1 \sigma_L) \pm Q_{\sigma_L, -\sigma_R}}{J\Delta}. \end{aligned}$$

Here $\sigma_{R(L)}$ stands for the value of the right (left) σ -spin for the given triangle.

After calculating the trace over the quantum degrees of freedom one arrives at the following expression for the partition function

$$\mathcal{Z} = \sum_{(\sigma)} \prod_{i=1}^L e^{\beta \frac{H_1}{2} (\sigma_i + \sigma_{i+1})} Z_{\sigma_i, \sigma_{i+1}} = \text{Tr} \mathbf{T}^L, \quad (9)$$

where \mathbf{T} is a 2×2 transfer matrix and $Z_{\sigma_i, \sigma_{i+1}}$ is the ‘‘partial’’ partition function of the i -th block:

$$Z_{\sigma_i, \sigma_{i+1}} = \text{Tr}_i e^{-\beta \mathcal{H}_i} = \sum_{n=1}^8 e^{-\beta \lambda_n(\sigma_i, \sigma_{i+1})}. \quad (10)$$

Substituting $\lambda_n(\sigma_i, \sigma_{i+1})$ from Eq. (6) one gets

$$\begin{aligned} Z_{\sigma_i, \sigma_{i+1}} &= 2 \left\{ e^{-\beta \frac{J_1 + 2J}{4}} \cosh \left(\beta \frac{3H_2 - K_1 \sigma_i - 2K_2 \sigma_{i+1}}{2} \right) + e^{\beta \frac{J_1(1 + 2\Delta_1)}{4}} \cosh \left(\frac{H_2 - K_1 \sigma_i}{2} \right) \right. \\ &\quad \left. + e^{-\beta \frac{J_1 \Delta_1 - J}{4}} \left[e^{\beta \frac{H_2 + K_2 \sigma_{i+1}}{2}} \cosh \left(\beta \frac{Q_{-\sigma_i, \sigma_{i+1}}}{4} \right) + e^{-\beta \frac{H_2 + K_2 \sigma_{i+1}}{2}} \cosh \left(\beta \frac{Q_{\sigma_i, -\sigma_{i+1}}}{4} \right) \right] \right\}. \end{aligned} \quad (11)$$

According to Eq. (9), the partial partition functions for

one block multiplied by the factor $e^{\beta \frac{H_1}{2} (\sigma_i + \sigma_{i+1})}$ yield the

entries of the transfer matrix for a certain block:

$$\mathbf{T} = \begin{pmatrix} e^{\beta \frac{H_1}{2}} Z_{\frac{1}{2}, \frac{1}{2}} & Z_{\frac{1}{2}, -\frac{1}{2}} \\ Z_{-\frac{1}{2}, \frac{1}{2}} & e^{-\beta \frac{H_1}{2}} Z_{-\frac{1}{2}, -\frac{1}{2}} \end{pmatrix}. \quad (12)$$

Thus, calculation of the partition function for the system

$$f = -\frac{1}{\beta} \ln \left[\frac{1}{2} \left(e^{\beta \frac{H_1}{2}} Z_{\frac{1}{2}, \frac{1}{2}} + e^{-\beta \frac{H_1}{2}} Z_{-\frac{1}{2}, -\frac{1}{2}} + \sqrt{\left(e^{\beta \frac{H_1}{2}} Z_{\frac{1}{2}, \frac{1}{2}} - e^{-\beta \frac{H_1}{2}} Z_{-\frac{1}{2}, -\frac{1}{2}} \right)^2 + 4 Z_{\frac{1}{2}, -\frac{1}{2}} Z_{-\frac{1}{2}, \frac{1}{2}}} \right) \right]. \quad (13)$$

Now it is straightforward to obtain not only all thermodynamic properties, but also expressions for the sublattice and total magnetizations:

$$\begin{aligned} M_\sigma &= \frac{2}{LZ} \sum_{(\sigma)} \text{Tr} \mathbf{S} \left(\sum_{i=1}^L \sigma_i e^{-\beta \mathcal{H}} \right) = -2 \left(\frac{\partial f}{\partial H_1} \right)_{\beta, H_2}, \\ M_S &= \frac{2}{3LZ} \sum_{(\sigma)} \text{Tr} \mathbf{S} \left(\sum_{i=1}^L \sum_{a=1}^3 (S_{i,a}^z) e^{-\beta \mathcal{H}} \right) \\ &= -\frac{2}{3} \left(\frac{\partial f}{\partial H_2} \right)_{\beta, H_1}, \\ M &= \frac{1}{2LZ} \sum_{(\sigma)} \text{Tr} \mathbf{S} \left(\sum_{i=1}^L \left(\sigma_i + \sum_{a=1}^3 (S_{i,a}^z) \right) e^{-\beta \mathcal{H}} \right) \\ &= \frac{1}{4} M_\sigma + \frac{3}{4} M_S. \end{aligned} \quad (14)$$

III. GROUND-STATE PROPERTIES

From the eigenvectors for one block of the system one can construct all possible ground states of the whole chain. The ground states of the system under consideration can be classified by the values of magnetization, M , which we normalize to saturation values ± 1 . In particular, one finds antiferromagnetic $M = 0$, ferrimagnetic ($M = 1/2$ or $1/4$), and ferromagnetic $M = 1$ ground states.

There are five ‘‘antiferromagnetic’’ ground states. Among them, there is a special one which is the closest analog of the fully dimerized ground state of the purely quantum orthogonal-dimer chain.^{28–30} However, in contrast to the latter, here the corresponding ground state exhibits a two-fold degeneracy per block due to the Ising-type interactions on the horizontal dimers. So, we will refer to this ground state as the *degenerate antiferromagnetic* state, which we will abbreviate by |AF1). In the state |AF1), the spins on vertical dimers form a perfect spin singlet, while the spins connected by a horizontal Ising bond are aligned antiparallel, but can freely change their overall orientation without changing the energy of the ground state. The corresponding wave func-

under consideration boils down to evaluating the trace of the L -th power of a 2 by 2 transfer matrix in full analogy with the ordinary Ising chain (see for example Refs. 1 and 32). The free energy per unit cell in the thermodynamic limit is obtained from the maximal eigenvalue of the transfer matrix (12):

tions read:

$$|\text{AF1}\rangle = \prod_{i=1}^L |v_{\pm \frac{1}{2}, a}, \mp\rangle_i. \quad (15)$$

Here, \mp stands for the ‘‘down’’ (‘‘up’’) orientation for the σ spin from the i -th block, which appears simultaneously with the $|v_{\frac{1}{2}, a}\rangle_i$ ($|v_{-\frac{1}{2}, a}\rangle_i$) configuration of the XXZ -triangle of the same block (compare Eq. (8) for the explicit form of $|v_{\pm \frac{1}{2}, a}\rangle_i$). It is worth mentioning, however, that the disentangled nature of the antiferromagnetic state of two spins connected by the Ising bond limits the analogy between the AF1 and the perfectly dimerized ground state of the purely quantum orthogonal-dimer chain. In particular, the two-fold degeneracy per block in our case has its origin in the above mentioned difference. Schematic figures illustrating the spin arrangement for the various ground states as well as their energies per block³³ can be found in Table I.

There is another $M = 0$ ground state with spatial period equal to the period of the system (four spins in the unit cell). This ground state corresponds to $S_{\text{tot}}^z = 1/2$ states of the quantum triangles which are aligned antiparallel with the $s = 1/2$ σ -spins between them:

$$|\text{AF2}\rangle = \prod_{i=1}^L |v_{\frac{1}{2}, s}^-, \downarrow\rangle_i. \quad (16)$$

Three further antiferromagnetic ground states are based on the eigenvectors of the triangular clusters which are asymmetric with respect to left and right σ -spins. These ground states break the translational symmetry spontaneously, leading to a doubling of the unit cell

$$\begin{aligned} |\text{AF3}\rangle &= \prod_{i=1}^{L/2} |v_{\frac{1}{2}, s}^-, \uparrow\rangle_{2i-1} |v_{-\frac{1}{2}, s}^-, \downarrow\rangle_{2i}, \\ |\text{AF4}\rangle &= \prod_{i=1}^{L/2} |v_{\frac{1}{2}, s}^-, \downarrow\rangle_{2i-1} |v_{-\frac{1}{2}, s}^-, \uparrow\rangle_{2i}, \\ |\text{AF5}\rangle &= \prod_{i=1}^{L/2} |v_{\frac{3}{2}, \uparrow}\rangle_{2i-1} |v_{-\frac{3}{2}, \downarrow}\rangle_{2i}. \end{aligned} \quad (17)$$

TABLE I. Ground states of the system and their energies per block.³³ The function Q is defined in Eq. (7). Vertical ellipses denote the quantum singlet state of the corresponding spins; horizontal rectangles denote a disordered pair of two Ising spins with $S_{\text{tot}} = 0$; gray triangles stand for the $|v_{\pm\frac{1}{2},s}^- \rangle$ ground states and a frame around a triangle indicates the degenerate superposition of $|v_{\frac{1}{2},s}^- \rangle$ and $|v_{\frac{1}{2},a}^- \rangle$. For more details compare the text.

Label	Energy per block	Spatial period	Figure
AF1	$-\frac{1}{4}(J_1(1+2\Delta_1)+K_1)$	undefined	
AF2	$-\frac{1}{4}(J-J_1\Delta_1+K_2+Q_{1/2,-1/2})$	1	
AF3	$-\frac{1}{4}(J-J_1\Delta_1+K_2+Q_{-1/2,-1/2})$	2	
AF4	$-\frac{1}{4}(J-J_1\Delta_1-K_2+Q_{1/2,1/2})$	2	
AF5	$\frac{1}{4}(J_1+2J-K_1+2K_2)$	2	
SM1	$-\frac{1}{4}(J-J_1\Delta_1+Q_{1/2,1/2}+Q_{-1/2,-1/2})-\frac{1}{2}H$	2	
SM2	$-\frac{1}{8}(J+J_1(1+\Delta_1)+K_1+K_2+Q_{-1/2,-1/2})-\frac{1}{2}H$	2	
SM3	$\frac{1}{4}(J-J_1\Delta_1-K_1+K_2)-\frac{1}{2}H$	2	
F1	$\frac{1}{4}(J_1+2J-K_1-2K_2)-H$	1	
F2	$-\frac{1}{4}(J_1(1+2\Delta_1)-K_1)-H$	1	
F3	$-\frac{1}{4}(J-J_1\Delta_1-K_2+Q_{-1/2,1/2})-H$	1	
F4	$-\frac{1}{4}(J(1+2\Delta)-K)-H$	undefined	
SP	$\frac{1}{4}(J_1+2J+K_1+2K_2)-2H$	1	

The $|\text{AF3}\rangle$ ground state is characterized by an antiferromagnetically ordered sublattice of triangles with $S_{\text{tot}}^z = \pm 1/2$ as well as by the same ordering of σ -spins. These two sublattices form an “up-up-down-down” overall arrangement of the local $s = 1/2$ magnetic moments. One can also notice that here we have an antiferromagnetic ordering of blocks with overall spin equal to ± 1 . In the $|\text{AF4}\rangle$ ground state, as in the previous case, one can see separate antiferromagnetic ordering of both σ -spins and triangles which are in the $s = 1/2$ state. However, inside each block they compensate each other (see Table I). In the $|\text{AF5}\rangle$ ground state one can see antiferromagnetic ordering of fully polarized blocks.

Now we turn to $M = 1/4$. Since this yields a fractional spin polarization per unit cell, $M = 1/4$ ground states are accompanied by spontaneous breaking of translational symmetry,^{31,34} more precisely, doubling of the unit cell. In view of the spatial modulation of the local spin polarization, we will refer to the corresponding ground states as spin modulated ones:

$$\begin{aligned} |\text{SM1}\rangle &= \prod_{i=1}^{L/2} |v_{\frac{1}{2},s}^-, \uparrow\rangle_{2i-1} |v_{\frac{1}{2},s}^-, \downarrow\rangle_{2i}, & (18) \\ |\text{SM2}\rangle &= \prod_{i=1}^{L/2} |v_{\frac{1}{2},s}^-, \uparrow\rangle_{2i-1} |v_{\frac{1}{2},a}^-, \downarrow\rangle_{2i}, \\ |\text{SM3}\rangle &= \prod_{i=1}^{L/2} |v_{\frac{3}{2}}^-, \uparrow\rangle_{2i-1} |v_{-\frac{1}{2},a}^-, \downarrow\rangle_{2i}. \end{aligned}$$

These ground states have more complicated local spin arrangements than the antiferromagnetic ones. In contrast to the latter, these “spin-modulated” ground states possess a doubled unit cell in which two blocks are not connected to each other by spin inversion (see Table I). Our model exhibits also three translationally invariant ferrimagnetic ground states with $M = 1/2$:

$$\begin{aligned} |\text{F1}\rangle &= \prod_{i=1}^L |v_{\frac{3}{2}}^-, \downarrow\rangle_i, & (19) \\ |\text{F2}\rangle &= \prod_{i=1}^L |v_{\frac{1}{2},a}^-, \uparrow\rangle_i, \\ |\text{F3}\rangle &= \prod_{i=1}^L |v_{\frac{1}{2},s}^-, \uparrow\rangle_i. \end{aligned}$$

Furthermore, there is also one family of ground states with a two-fold degeneracy per block with $M = 1/2$ in which all σ spins point up, while the quantum triangles can freely and independently oscillate between $|v_{\frac{1}{2},a}^-\rangle$ and $|v_{\frac{1}{2},s}^-\rangle$. However, these ground states appear only for the highly symmetric choice of parameters $\Delta = \Delta_1$, $J = J_1$, $K_1 = K_2$. The corresponding eigenvectors are

$$|\text{F4}\rangle = \prod_{i=1}^L |V_{\frac{1}{2}}^-, \uparrow\rangle_i, \quad (20)$$

TABLE II. Equations of the phase boundaries for $J = J_1 > 0$, $K_1 = K_2 \equiv K$, and $\Delta = \Delta_1$ (corresponding to the top panel of Fig. 2). The abbreviations q and \bar{q} are introduced in Eq. (22).

Phase 1	Phase 2	Boundary
AF4	SP	$h = \frac{1}{8}(4 - \Delta + 2\kappa + q(-\kappa))$
AF4	F4	$h = \frac{1}{4}(-3\Delta + q(-\kappa))$
F4	SP	$h = \frac{1}{2}(2 + \Delta + \kappa)$
SM2	F4	$h = \frac{1}{4}(-3\Delta + 4\kappa + q(\kappa))$
AF3	SM2	$h = \frac{1}{4}(-3\Delta - 2 + q(-\kappa))$
SM2	F1	$h = \frac{1}{4}(8 + \Delta_1 - 4\kappa + q(-\kappa))$
AF3	F1	$h = \frac{1}{4}(4 - \Delta - 2\kappa q(-\kappa))$
F1	SP	$h = \frac{3}{2}\kappa$
F4	F1	$\kappa = 1 + \frac{1}{2}\Delta$

where $|V_{\frac{1}{2}}^-\rangle$ can be either one of the states $|v_{\frac{1}{2},a}^-\rangle$ or $|v_{\frac{1}{2},s}^-\rangle$. Finally, there is the fully polarized ground state

$$|\text{SP}\rangle = \prod_{i=1}^L |v_{\frac{3}{2}}^-, \uparrow\rangle_i. \quad (21)$$

IV. GROUND-STATE PHASE DIAGRAMS

Ground-state phase diagrams can be derived from the energies of the ground states given in Table I. Since there are many free parameters, one needs to make some choices and it is natural to set certain exchange constants equal. We are going to focus on two cases. The first one corresponds to a situation with one exchange constant for all quantum bonds and another one for all Ising bonds ($J = J_1 \equiv J$, $K_1 = K_2 \equiv K$) while the anisotropy constants for the two types of quantum bonds can still be different. The other case is well investigated in the context of the quantum orthogonal-dimer chain,²⁸⁻³¹ where there are two interaction parameters, one for vertical and horizontal dimers, and another one for diagonal bonds ($K_1 = J_1 \equiv \tilde{J}$, $K_2 = J \equiv K$).

A. $J = J_1$, $K_1 = K_2 \equiv K$

Analyzing $T = 0$ properties of the system under consideration one can find a rich variety of possible ground states. First of all, one can distinguish cases of ferromagnetic and antiferromagnetic J . Hereafter, we will measure all coupling constants in units of $|J|$.

In the antiferromagnetic region $J > 0$ we observe a strong dependence on the ratio of Δ/Δ_1 . For equal anisotropy in the triangles ($\Delta = \Delta_1$), the system exhibits an exceptional macroscopically degenerate ferrimagnetic ground state with $M = 1/2$, $|\text{F4}\rangle$. The top panel of Fig. 2 presents the phase diagram for $J > 0$ and $\Delta = \Delta_1$. This phase diagram has a point ($K = 0$, $H = 0$) where four

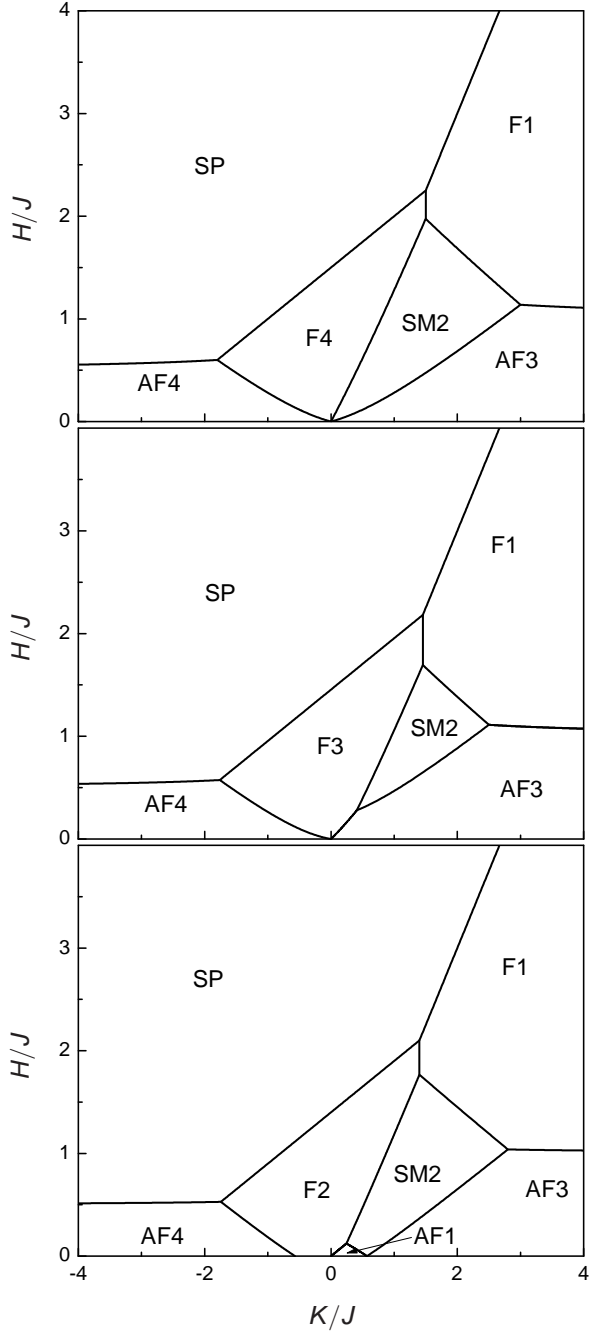


FIG. 2. Ground-state phase diagrams for antiferromagnetic $J_1 = J > 0$ and $K_1 = K_2 \equiv K$. The top panel shows the case of isotropic interaction ($\Delta = \Delta_1 = 1$). A characteristic feature is the appearance of the macroscopically degenerate ferrimagnetic phase F4 with $M = 1/2$. The lower two panels show the case of Ising-like anisotropies, namely $\Delta = 0.8 > \Delta_1 = 0.5$ (middle panel) and $\Delta = 0.5 < \Delta_1 = 0.8$ (lowest panel). Note that Δ and Δ_1 are the prefactors of the XY -term in the spin Hamiltonian.

ground states merge, with a very high (eight-fold) degeneracy per block. However, the origin of this degeneracy is trivial, as the system at such values of parameters is

TABLE III. Equations of the phase boundaries for $J = J_1 > 0$, $K_1 = K_2 \equiv K$, and $\Delta > \Delta_1$ (corresponding to the middle panel of Fig. 2).

Phase 1	Phase 2	Boundary
AF4	SP	$h = \frac{1}{8}(4 - \Delta_1 + 2\kappa + q(-\kappa))$
AF4	F3	$h = \frac{1}{4}(q(-\kappa) - q(0))$
F3	SP	$h = \frac{1}{4}(4 - \Delta_1 + 2\kappa + q(0))$
AF3	F3	$h = \frac{1}{4}(2\kappa - q(0) + q(\kappa))$
AF3	F1	$h = \frac{1}{4}(4 - \Delta_1 - 2\kappa + q(\kappa))$
AF3	SM2	$h = \frac{1}{4}(-3\Delta_1 + q(\kappa))$
SM2	F3	$h = \frac{1}{4}(3\Delta_1 + 4\kappa - 2q(0) + q(\kappa))$
SM2	F1	$h = \frac{1}{4}(8 + \Delta_1 - 4\kappa + q(\kappa))$
F1	SP	$h = \frac{3}{2}\kappa$
F3	F1	$\kappa = 1 - \frac{1}{4}(\Delta_1 - q(0))$

TABLE IV. Additional equations of the phase boundaries for $J = J_1 > 0$, $K_1 = K_2 \equiv K$, and $\Delta_1 > \Delta$ (corresponding to the lower panel of Fig. 2). The other equations of phase boundaries are the same as in Table III.

Phase 1	Phase 2	Boundary
AF4	F2	$h = \frac{1}{4}(-3\Delta_1 + q(-\kappa))$
F2	SP	$h = \frac{1}{2}(2 + \Delta_1 + \kappa)$
F2	AF1	$h = \frac{1}{2}\kappa$
AF1	SM2	$h = \frac{1}{4}(3\Delta_1 - q(\kappa))$
SM2	F2	$h = \frac{1}{4}(-3\Delta_1 + 4\kappa + q(\kappa))$
F1	F2	$\kappa = 1 + \frac{1}{4}\Delta_1$

just a set of triangles and single spins decoupled from each other. One also observes antiferromagnetic ($M = 0$) and ferrimagnetic spatially modulated ($M = 1/2$) ground states. The equations of the corresponding phase boundaries are listed in Table II. Here and below we use the following notations:

$$\begin{aligned}
 q(x) &= \sqrt{8\Delta^2 + (\Delta_1 + 2x)^2}, \\
 \bar{q}(x) &= \sqrt{8\Delta^2 + (\Delta + 2x)^2}, \\
 q_\kappa(x) &= \sqrt{8\Delta^2\kappa^2 + (\Delta_1 + 2x)^2}, \\
 \bar{q}_\kappa(x) &= \sqrt{8\Delta^2\kappa^2 + (\Delta + 2x)^2}.
 \end{aligned} \tag{22}$$

Throughout this section we use the abbreviations $\kappa = K/|J|$ and $h = H/|J|$.

The middle panel of Fig. 2 presents the phase diagram for $\Delta/\Delta_1 > 1$. Depending on the value of the ratio $\kappa = K/J$ and the magnetic field measured in units of J ($h = H/J$), the system exhibits two antiferromagnetic, two ferrimagnetic, and one spin-modulated ground state, apart from the spin-polarized one. The present ground-state phase diagram differs from the previous one (see Fig. 2, top panel). Here, the degenerate ferrimagnetic ground state |F4⟩ is replaced by |F3⟩ and the region corresponding to |SM2⟩ is smaller than in the previous case. An interesting feature of the symmetry breaking imposed by the distinct values of the anisotropy is the disappearance of the points where four phases merge. The equations for the corresponding phase boundaries

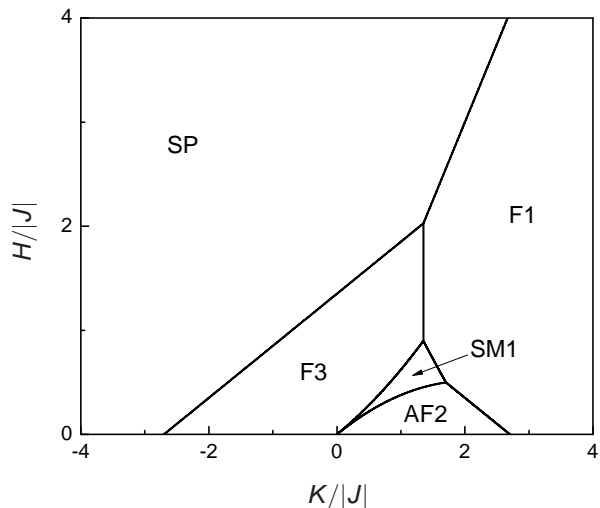


FIG. 3. Ground-state phase diagram for the case of ferromagnetic $J_1 = J < 0$, $K_1 = K_2 \equiv K$, and $\Delta = 2$, $\Delta_1 = 3$ (XY-like anisotropy).

TABLE V. Equations of phase boundaries for ferromagnetic $J = J_1 < 0$ and $K_1 = K_2 \equiv K$ (Fig. 3).

Phase 1	Phase 2	Boundary
F3	SP	$h = \frac{1}{4}(\Delta_1 - 4 + 2\kappa + q(0))$
AF2	SM1	$h = \frac{1}{4}(2\kappa + 2q(0) - q(-\kappa) - q(\kappa))$
SM1	F3	$h = \frac{1}{4}(2\kappa - 2q(0) + q(-\kappa) + q(\kappa))$
SM1	F1	$h = \frac{1}{4}(-6\kappa + 2\Delta_1 - 8 + q(-\kappa) + q(\kappa))$
AF2	F1	$h = \frac{1}{4}(\Delta_1 - 4 - 2\kappa + q(0))$
F1	SP	$h = \frac{3}{2}\kappa$

can be found in Table III.

The lower panel of Fig. 2 presents the phase diagram for the opposite relation between anisotropy constants $\Delta/\Delta_1 < 1$ and antiferromagnetic $J > 0$. Here one new feature arises. Namely, one observes the macroscopically degenerate antiferromagnetic ground state $|\text{AF1}\rangle$ between the $|\text{F2}\rangle$ and $|\text{SM2}\rangle$ states. Table IV contains the equations for all phase boundaries.

Finally, for ferromagnetic $J < 0$ one finds the phase diagram shown in Fig. 3. The corresponding equations of phase boundaries are listed in Table V.

All phase transitions in Figs. 2 and 3 correspond to level crossings and thus should be considered as first-order transitions.

B. $J_1 = K_1 \equiv \tilde{J}$, $J = K_2 \equiv K$

The case where dimers have one coupling constant $J_1 = K_1 \equiv \tilde{J}$ and diagonal bonds another one $J = K_2 \equiv K$ is the closest analog of the conventional purely quantum orthogonal-dimer chain. The ground state phase diagrams for this case are presented in Fig. 4.

As before, one should distinguish ferromagnetic and

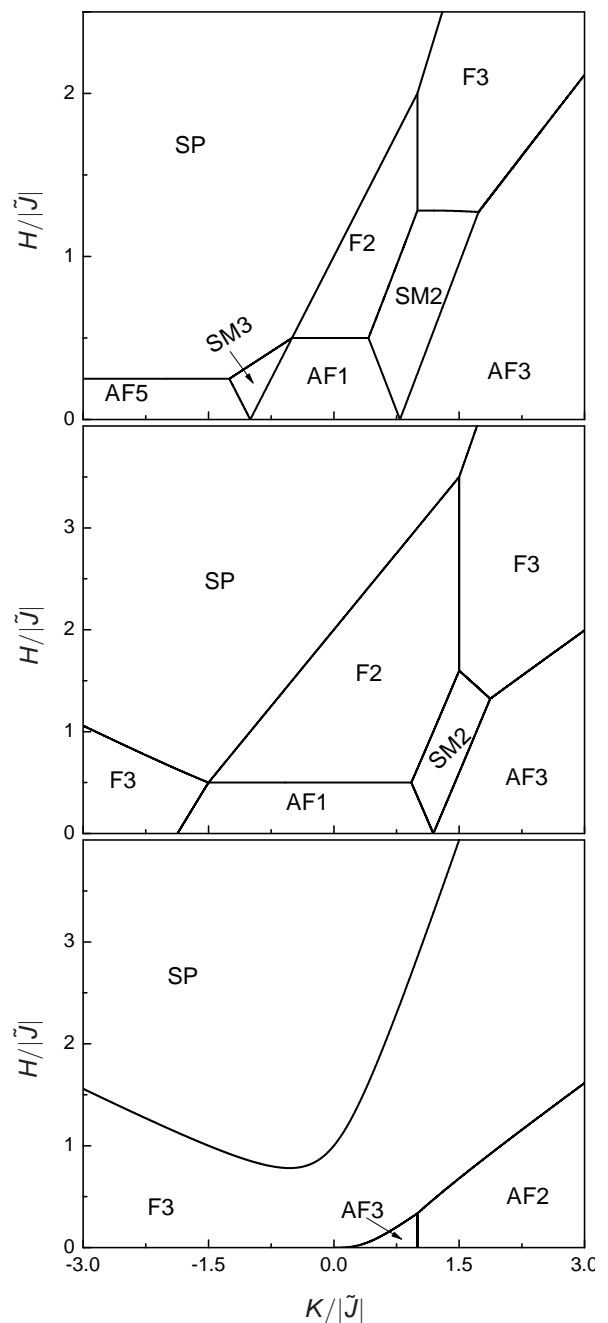


FIG. 4. Ground-state phase diagrams for the case $J = K_2 \equiv K$, $J_1 = K_1 \equiv \tilde{J}$, which corresponds most closely to the fully quantum orthogonal-dimer chain. The top panel corresponds to isotropic interactions inside the triangles, $\Delta = \Delta_1 = 1$, and antiferromagnetic $\tilde{J} > 0$. The middle (lower) panel shows the case of antiferromagnetic (ferromagnetic) \tilde{J} for the anisotropic case $\Delta = 2$, $\Delta_1 = 3$ (XY-like anisotropy).

antiferromagnetic regions of \tilde{J} . In both cases, the appearance of different ground states is affected by the ratio Δ/Δ_1 . The richest phase diagram exhibiting eight ground states corresponds to the isotropic case $\Delta = \Delta_1$ and is shown in the top panel of Fig. 4. One observes

TABLE VI. Equations of the phase boundaries for the case $J_1 = K_1 \equiv \tilde{J} > 0$, $J = K_2 \equiv K$ and isotropic interaction inside triangles $\Delta = \Delta_1 = 1$ (Fig. 4, top panel).

Phase 1	Phase 2	Boundary
AF5	SP	$h = \frac{1}{4}$
AF5	SM3	$h = -\frac{1}{2}(1 + \Delta + 2\kappa)$
SM3	SP	$h = \frac{1}{6}(3 + \Delta + 2\kappa)$
AF1	SM3	$h = \frac{1}{3}(1 + \Delta + 2\kappa)$
AF1	F2	$h = \frac{1}{2}$
F2	SP	$h = \frac{1}{2}(1 + \Delta + 2\kappa)$
AF1	SM2	$h = \frac{1}{4}(2 + 3\Delta - 2\kappa - \overline{q_\kappa}(\kappa))$
SM2	F2	$h = \frac{1}{4}(2 - 3\Delta + 2\kappa + \overline{q_\kappa}(\kappa))$
AF3	SM2	$h = \frac{1}{4}(-2 - 3\Delta + 2\kappa + \overline{q_\kappa}(\kappa))$
SM2	F3	$h = \frac{1}{4}(2 + 3\Delta + 2\kappa - 2\Delta\overline{q_\kappa}(0) + \overline{q_\kappa}(\kappa))$
SM2	F2	$h = \frac{1}{4}(2 - 3\Delta + 2\kappa + \overline{q_\kappa}(\kappa))$
F3	F2	$\kappa = 1$
AF3	F3	$h = \frac{1}{4}(2\kappa - \Delta\overline{q_\kappa}(0) + \overline{q_\kappa}(\kappa))$
F3	SP	$h = \frac{1}{4}(2 - \Delta + 4\kappa + \Delta\overline{q_\kappa}(0))$

TABLE VII. Equations of the phase boundaries for the case $J_1 = K_1 \equiv \tilde{J} > 0$, $J = K_2 \equiv K$, and $\Delta = 2$, $\Delta_1 = 3$ (Fig. 4 middle panel).

Phase 1	Phase 2	Boundary
F3	SP	$h = \frac{1}{4}(4\kappa - \Delta_1 + 2 + q_\kappa(0))$
F3	AF1	$h = \frac{1}{4}(2 + 3\Delta_1 - q_\kappa(0))$
AF1	F2	$h = \frac{1}{2}$
F2	SP	$h = \frac{1}{2}(1 + \Delta_1 + 2\kappa)$
AF1	SM2	$h = \frac{1}{4}(2 + 3\Delta_1 - 2\kappa - q_\kappa(\kappa))$
SM2	F2	$h = \frac{1}{4}(2 - 3\Delta_1 + 2\kappa + q_\kappa(\kappa))$
SM2	AF3	$h = \frac{1}{4}(-2 - 3\Delta_1 + 2\kappa + q_\kappa(\kappa))$
SM2	F3	$h = \frac{1}{4}(2 + 3\Delta_1 + 2\kappa - 2q_\kappa(0) + q_\kappa(\kappa))$
AF3	F3	$h = \frac{1}{4}(2\kappa - q_\kappa(0) + q_\kappa(\kappa))$
F3	SP	$h = \frac{1}{4}(1 - \Delta_1 + 5\kappa + q_\kappa(0))$
F2	F3	$\kappa = \Delta_1/\Delta$

a broad region corresponding to the macroscopically degenerate antiferromagnetic ground state $|AF1\rangle$ which is the closest analog of the exact dimerized ground state of the purely quantum orthogonal-dimer chain.^{28–30} The system also exhibits four ground states with period doubling, $|AF3\rangle$, $|AF5\rangle$, $|SM2\rangle$, and $|SM3\rangle$. It is worth mentioning that there is a point where the four ground states $|SM3\rangle$, $|AF1\rangle$, $|F2\rangle$, and $|SP\rangle$ become degenerate, which implies a large entropy accumulation. For the isotropic case ($\Delta = \Delta_1 = 1$) presented in the top panel of Fig. 4, the position of this point is $K/\tilde{J} = -1/2$, $H/\tilde{J} = 1/2$ and the corresponding entropy per unit cell is $S/L = 1.44364$. The equations of the phase boundaries can be found in Table VI. Throughout this section we use the abbreviations $\kappa = K/|\tilde{J}|$ and $h = H/|\tilde{J}|$.

The structure of the phase diagram for anisotropic interactions and antiferromagnetic \tilde{J} , $K > 0$ is qualitatively similar. The middle panel of Fig. 4 shows the ground state phase diagram for $\Delta = 2$, $\Delta_1 = 3$, and $\tilde{J} > 0$. Here one can see that, in comparison with the isotropic case, there is no region corresponding to the $|SM3\rangle$ state

TABLE VIII. Equations of phase boundaries for ferromagnetic $J_1 = K_1 \equiv \tilde{J} < 0$ and $J = K_2 \equiv K$ (lower panel of Fig. 4).

Phase 1	Phase 2	Boundary
F3	SP	$h = \frac{1}{4}(4\kappa + \Delta_1 + q_\kappa(0))$
AF3	F3	$h = \frac{1}{4}(2\kappa - q_\kappa(0) + q_\kappa(-\kappa))$
AF2	F3	$h = \frac{1}{4}(2\kappa - q_\kappa(0) + q_\kappa(-\kappa - 1))$
AF2	AF3	$\kappa = \frac{1}{2}(\Delta_1 - 1)$

and the antiferromagnetic $|AF5\rangle$ ground state is replaced by the ferrimagnetic state $|F3\rangle$. Still, there is a point of large entropy accumulation where four ground states $|F3\rangle$, $|AF1\rangle$, $|F2\rangle$, and $|SP\rangle$ become degenerate. In the symmetric but anisotropic case $\Delta = \Delta_1 \neq 1$, the value of the entropy at the corresponding point is $S/L = 1.60944$, corresponding to a five-fold degeneracy per block. Note also the line of degeneracy between the $|F2\rangle$ and $|F3\rangle$ states which one can see both in the top and middle panel of Fig. 4. This line is at $K/\tilde{J} = \Delta_1/\Delta$ and corresponds to the degenerate $|F4\rangle$ ground state which in some sense is a superposition of $|F2\rangle$ and $|F3\rangle$.

Lastly, the region of ferromagnetic $\tilde{J} < 0$ is quite different. The lower panel of Fig. 4 demonstrates the ground-state phase diagram for ferromagnetic \tilde{J} and asymmetric anisotropic couplings $\Delta = 2$, $\Delta_1 = 3$. The equations of the phase boundaries corresponding to the middle and lower panels of Fig. 4 are listed in Tables VII and VIII, respectively.

Again, all phase transitions in Fig. 4 are first-order transitions in the sense that they correspond to level crossings.

V. MAGNETIZATION PROCESS

The phase diagrams show that the model (1), (2) exhibits a large diversity of magnetic behaviors. Namely, depending on the values of parameters, the following step-like transitions between plateaux in the magnetization curves can be observed when the magnetic field is varied from zero to the saturation value: $M = 0 \rightarrow 1$, $M = 0 \rightarrow 1/2 \rightarrow 1$, $M = 0 \rightarrow 1/4 \rightarrow 1/2 \rightarrow 1$, $M = 0 \rightarrow 1/4 \rightarrow 1$, $M = 1/2 \rightarrow 1$, and $M = 1/4 \rightarrow 1/2 \rightarrow 1$. As there are no excitation bands in the model, all transitions between different ground states are strictly step-like at $T = 0$.

Here we illustrate some variants of the magnetization process and demonstrate the effect of a finite temperature using the exact solution of the model. For sufficiently low temperatures, the form of the magnetization curve almost coincides with the zero-temperature limit. Further details for $T = 0$ will be given in the comparison with the full quantum mechanical Heisenberg model in Section VI B below.

Fig. 5 shows the magnetization curve for the most symmetric case $J = J_1 = K_1 = K_2 = 1$ and $\Delta = \Delta_1 = 1$,

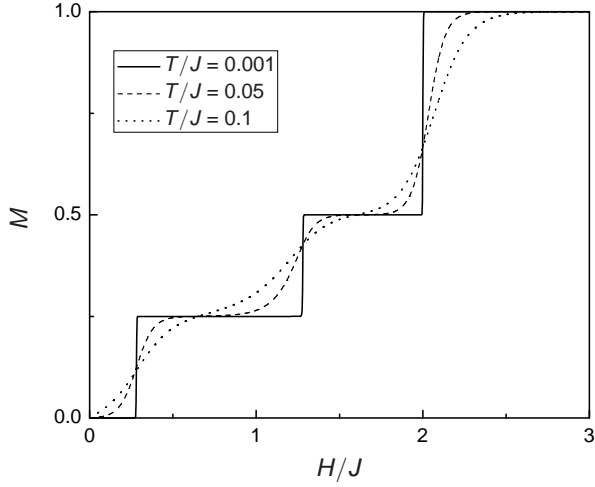


FIG. 5. Magnetization curve for $J_1 = K_1 = 1$, $J = K_2 = 1$, and $\Delta = \Delta_1 = 1$. The corresponding ground states can be seen both in the top panel of Fig. 2 and the top panel of Fig. 4. For very low temperature (solid line) the sequence of step-like transitions between the corresponding ground states is recovered. Dashed and dotted lines correspond to $T/J = 0.05$ and $T/J = 0.1$, respectively.

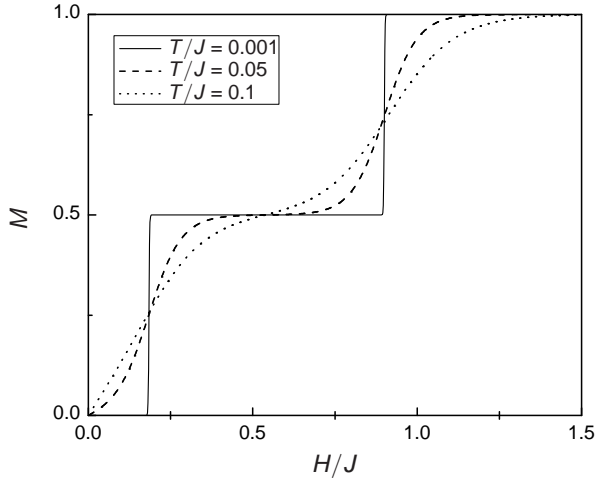


FIG. 6. Magnetization curve for $J = J_1 = 1$, $K_1 = K_2 = -1$, and $\Delta = 0.5$, $\Delta_1 = 0.8$ (Ising-like anisotropy). The solid line corresponding to $T/J = 0.001$ shows sharp transitions between three plateaux: $M = 0$, $1/2$, and 1 . Dashed and dotted lines correspond to $T/J = 0.05$ and $T/J = 0.1$, respectively.

for $T/J = 0.001$, 0.05 , and 0.1 . One can see here a sequence of magnetization plateaux corresponding to the following transitions between the ground states at $T = 0$: $|\text{AF3}\rangle \rightarrow |\text{SM2}\rangle \rightarrow |\text{F4}\rangle \rightarrow |\text{SP}\rangle$ which corresponds to both phase diagrams from Fig. 2 and Fig. 4. The line $K/\tilde{J} = 1$ from the upper panel of Fig. 4 where $|\text{F2}\rangle$ and $|\text{F3}\rangle$ become degenerate corresponds to the degenerate $|\text{F4}\rangle$ ground state.

Fig. 6 exhibits another form of magnetic behavior with

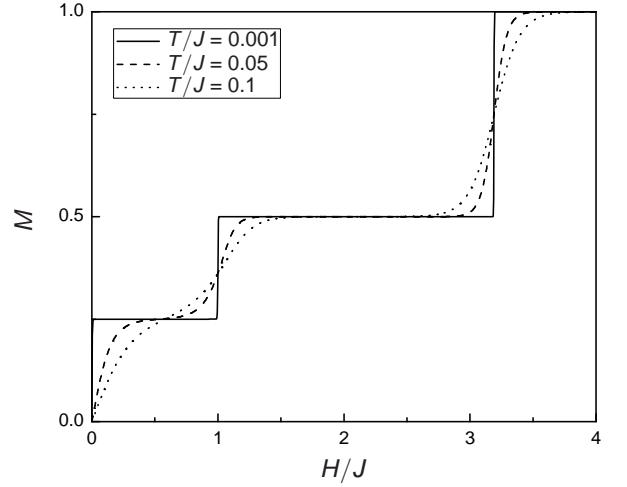


FIG. 7. Magnetization curve for $J_1 = K_1 = 1$, $J = K_2 = 1.19034$, and $\Delta = 2$, $\Delta_1 = 3$ (XY-like anisotropy). The solid line corresponds to $T/J = 0.001$ and shows sharp transitions between three plateaux: $M = 1/4$, $1/2$, and 1 . Dashed and dotted lines correspond to $T/J = 0.05$ and $T/J = 0.1$, respectively.

only two intermediate plateaux at $M = 0$ and $1/2$, respectively. For the values of parameters corresponding to the figure ($J = J_1 = 1$, $K_1 = K_2 = -1$ and $\Delta = 0.5$, $\Delta_1 = 0.8$), these plateaux correspond to the $|\text{AF4}\rangle$ and $|\text{F2}\rangle$ ground states (see lower panel of Fig. 2).

Fig. 7 shows the magnetization curves for $J_1 = K_1 = 1$, $J = K_2 = 1.19034$ and $\Delta = 2$, $\Delta_1 = 3$ which corresponds to the middle panel of Fig. 4. This exceptional value of K/\tilde{J} corresponds to the point of the phase diagram where the three ground states $|\text{AF1}\rangle$, $|\text{SM2}\rangle$, and $|\text{F3}\rangle$ become degenerate, ($K/\tilde{J} = \frac{1}{16}(-14 + 2\sqrt{273})$, $H = 0$) and the first plateau in the magnetization curve corresponds to $M = 1/4$.

VI. HEISENBERG MODEL

In the following we would like to test to which extent the reduction to Ising interactions for certain bonds affects the properties of the model. For this purpose we will use the Heisenberg-Ising variant of the model (1), (2), *i.e.*, we will put $\Delta = \Delta_1 = 1$.

The comparison will be carried out with the Heisenberg analog of the Hamiltonian

$$\mathcal{H} = \sum_{i=1}^{N/4} \left(J \mathbf{S}_{i,1} \cdot (\mathbf{S}_{i,2} + \mathbf{S}_{i,3}) + J_1 \mathbf{S}_{i,2} \cdot \mathbf{S}_{i,3} + K_1 \mathbf{S}_{i,1} \cdot \mathbf{S}_{i,4} + K_2 (\mathbf{S}_{i,2} + \mathbf{S}_{i,3}) \cdot \mathbf{S}_{i+1,4} - H \sum_{a=1}^4 S_{i,a}^z \right). \quad (23)$$

Note that we have replaced the Ising spin σ_i in Eqs. (1),

(2) with a full $s = 1/2$ Heisenberg spin $\mathbf{S}_{i,4}$.

A. Method

Firstly, one can use conservation of the total $S^z = \sum_{i,a} S_{i,a}^z$ to relate the energy $E(S^z, H)$ in a magnetic field to that at zero field

$$E(S^z, H) = E(S^z, 0) - H S^z. \quad (24)$$

It is therefore sufficient to diagonalize (23) in a given sector of S^z for $H = 0$.

Secondly, we can introduce composite operators

$$\mathbf{T}_i = \mathbf{S}_{i,2} + \mathbf{S}_{i,3} \quad (25)$$

and rewrite the $H = 0$ case of (23) as follows:

$$\mathcal{H}_{H=0} = \sum_{i=1}^{N/4} \left(J \mathbf{S}_{i,1} \cdot \mathbf{T}_i + J_1 \left(\mathbf{T}_i^2 - \frac{3}{2} \right) + K_1 \mathbf{S}_{i,1} \cdot \mathbf{S}_{i,4} + K_2 \mathbf{T}_i \cdot \mathbf{S}_{i+1,4} \right). \quad (26)$$

This puts our model into the class of one-dimensional models with local conservation laws.^{12,13,18,28–31,35–57} This property can be used to simplify the diagonalization: Since the total spin \mathbf{T}_i on each vertical dimer is separately conserved, diagonalization of (23) is reduced to diagonalization of (26) for all possible combinations $T_i = 0, 1$ (with $\mathbf{T}_i^2 = T_i(T_i + 1)$). In fact, a singlet $T_i = 0$ splits the chain into “fragments”: all states for a given singlet pattern are product states of the corresponding eigenstates of the open fragments separated by these singlets. Hence, it is sufficient to diagonalize all open fragments with up to $N/4 - 1$ blocks in which $T_i = 1$ and one periodic system with $N/4$ with all $T_i = 1$ in order to obtain the spectrum for a periodic chain with N sites.^{49,55} For $K_2 = J$, the use of reflection symmetry allows us to fully diagonalize a system with $N = 24$ spins $1/2$, a task which in view of the large unit cell of the model would be very demanding if not impossible for the original Hamiltonian (23).

Ground states consist of a periodic repetition of one fragment of a certain length or a periodic system of a given length with all $T_i = 1$.³⁰ In the former case, we can construct the exact thermodynamic limit of the magnetization curves, provided that we have access to sufficiently long fragments. For the periodic system, we use (i) values for plateau boundaries obtained at sufficiently large N and (ii) the standard midpoint method^{58,59} as applied to the largest available system size to approximate the thermodynamic limit in smooth regions of the magnetization curve.

The main limitation for the computation of ground-state properties is the diagonalization of a periodic system with all $T_i = 1$. To push this a bit further, we

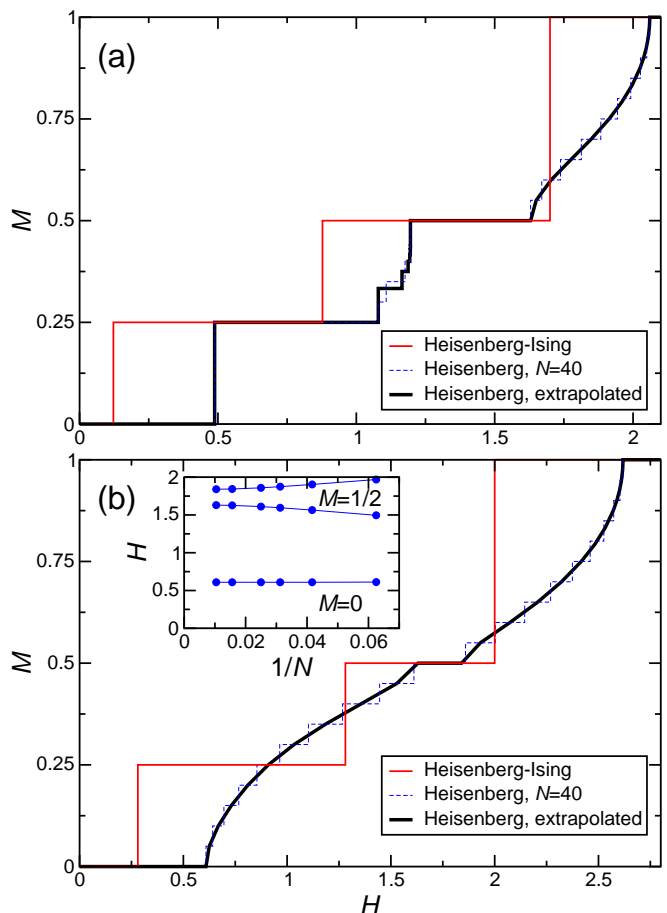


FIG. 8. (Color online) Zero-temperature magnetization curves for two cases where all exchange constants are antiferromagnetic: $J_1 = K_1 = 1, J = K_2 = 0.7$ (a) and $J_1 = J = K_1 = K_2 = 1$ (b). Dashed lines show numerical results for a Heisenberg chain with $N = 40$ spins $1/2$ and thick full lines an extrapolation to the thermodynamic limit. Thin full lines show the exact solution of the Heisenberg-Ising model in the thermodynamic limit $N = \infty$. The inset of panel (b) shows the finite-size behavior of the edge of the $M = 0$ plateau (spin gap) and the two edges of the $M = 1/2$ plateau at $J_1 = J = K_1 = K_2 = 1$.

have used the ALPS 1.3 implementation⁶⁰ of the density-matrix renormalization group (DMRG) method.^{61,62} Below we show results based on DMRG for $N = 40$ in the regime $M < 1/2$ and $N = 64$ with $m = 400$ kept states as well as $N = 96$ with $m = 600$ kept states. In the case $J_1 = J = 1, K_1 = K_2 = -1$, we have exceptionally increased the number of kept states to $m = 600$ and 800 for $N = 64$ and 96 , respectively. We have always also performed computations with lower m to ensure convergence of the data.

TABLE IX. Local spin polarizations on the $M = 1/4$ plateau for $J_1 = K_1 = 1$, $J = K_2 = 0.7$ (see Fig. 8(a)).

	Heisenberg	Heisenberg-Ising
$S_{i,1}^z$	0.3312	0.5
$S_{i,2}^z + S_{i,3}^z (= T_i^z)$	0	0
$S_{i+1,4}^z / \sigma_{i+1}$	0.3312	-0.5
$S_{i+1,1}^z$	-0.2237	-0.1022
$S_{i+1,2}^z + S_{i+1,3}^z (= T_{i+1}^z)$	0.7849	0.6022
$S_{i+2,4}^z / \sigma_{i+2}$	-0.2237	0.5

B. Magnetization curves

Now we present examples of numerical results for magnetization curves of the Heisenberg model (23) and compare them with the Heisenberg-Ising model (1), (2) with $\Delta = \Delta_1 = 1$.

1. $J_1 = K_1 = 1$, $J = K_2 = 0.7$

Fig. 8(a) shows the case $J_1 = K_1 = 1$, $J = K_2 = 0.7$ which has been discussed previously.²⁹⁻³¹ Our new exact diagonalization results agree with the previous ones. Note that the spin-1/2 Heisenberg model most likely gives rise to an infinite sequence of magnetization plateaux which accumulate just below $M = 1/2$.³⁰ This infinite sequence of plateaux is not reproduced by the Heisenberg-Ising model (red thin full line in Fig. 8(a)) which does, however, reproduce some of the most prominent features: (i) a spin gap at $M = 0$, (ii) two broad plateaux at $M = 1/4$ and $1/2$, and (iii) a jump from $M = 0$ to $1/4$. This choice of parameters corresponds to a cut through the top panel of Fig. 4 at $K/\tilde{J} = 0.7$ such that one can read off the corresponding ground states of the Heisenberg-Ising model.

For $M = 0$, the ground state of the Heisenberg model is characterized by all $T_i = 0$. This leaves isolated horizontal dimers which also form singlets. The corresponding ground state of the Heisenberg-Ising model is the |AF1) state. This is in fact the closest analog of the fully dimerized ground state: the vertical dimers are also in the singlet state for the |AF1) state. However, due to the missing quantum fluctuations the horizontal dimer bond is unable to form a singlet. The two local classical antiparallel spin configurations appear both with equal probability in the |AF1) state instead of forming a singlet superposition. This also gives rise to a macroscopic ground-state degeneracy of the Heisenberg-Ising model with entropy $S/L = \ln 2$ per unit cell.

For $M = 1/4$, $T_i = 0$ and 1 alternate in the ground state of the Heisenberg model, *i.e.*, the ground state breaks translational symmetry spontaneously. The same translational symmetry breaking is observed in the corresponding |SM2) state of the Heisenberg-Ising model. A more detailed comparison of the two states is given by the local spin polarizations along the field direction shown in

Table IX. For the Heisenberg model, this follows from the local expectation values in the $S^z = 1$ sector of a fragment consisting of a single block. For the Heisenberg-Ising model one needs instead the expectation values in the $|v_{\frac{1}{2},s}^- \rangle$ state of a single quantum triangle. Using the explicit form of the eigenvector given in Eq. (8) one arrives at

$$\langle v_{\frac{1}{2},s}^- | (S_2^z + S_3^z) | v_{\frac{1}{2},s}^- \rangle = \frac{c_-^2}{2 + c_-^2}, \quad (27)$$

$$\langle v_{\frac{1}{2},s}^- | S_1^z | v_{\frac{1}{2},s}^- \rangle = \frac{1 - \frac{1}{2}c_-^2}{2 + c_-^2}.$$

Combination with the |SM2) wave function given in Eq. (18) yields the corresponding entries in Table IX. The entries in Table IX exhibit a similar structure of the $M = 1/4$ state at $J_1 = K_1 = 1$, $J = K_2 = 0.7$ in the Heisenberg and Heisenberg-Ising models. In particular, vertical dimers in the singlet state alternate with predominantly polarized ones. The quantitative differences observed in Table IX can be attributed to the interaction of the Heisenberg-Ising model breaking the spatial reflection symmetry of the Heisenberg model.

In the $M = 1/2$ state of the Heisenberg model one finds all vertical dimers in the state $T_i = 1$. This state is non-degenerate and thus translationally invariant. The spin polarizations in this state have to be determined numerically; using DMRG one finds $S_{i,1}^z = S_{i,4}^z = 0.0640$ and $S_{i,2}^z + S_{i,3}^z = T_i^z = 0.8721$.⁶³ The corresponding ground state of the Heisenberg-Ising model is the |F2) state. Accordingly, the spin polarizations are read off from Eq. (19) as $S_{i,1}^z = \sigma_i = 1/2$ and $S_{i,2}^z + S_{i,3}^z = 0$. So, in this case the difference between the Heisenberg model and the Heisenberg-Ising model is bigger although the $M = 1/2$ ground states still have the same translational symmetry.

2. $J_1 = J = K_1 = K_2 = 1$

The effect of increasing $J = K_2$ from 0.7 to 1 is demonstrated in Fig. 8(b). The magnetization curve of the Heisenberg-Ising-model (which was in fact already presented in Fig. 5) remains similar to the one in Fig. 8(a). However, some of the plateau states of the Heisenberg-Ising-model change; the sequence is now |AF3) \rightarrow |SM2) \rightarrow |F3) \rightarrow |SP) (see top panel of Fig. 4). The Heisenberg model still has a spin gap at $M = 0$, but its state is also changed: now it arises out of a periodic system with all $T_i = 1$, as already observed in Ref. 44. The $M = 1/2$ state of the Heisenberg model also corresponds to all $T_i = 1$ and is non-degenerate. Since in this case finite-size effects are important at $M = 1/2$, we have performed a finite-size analysis which is shown in the inset of Fig. 8(b). While the width of the $M = 1/2$ plateau initially shrinks with growing N , $N = 96$ is a good approximation to the thermodynamic limit $1/N = 0$. In

TABLE X. Values of local spin polarizations for the ground states corresponding to the magnetization plateaux in Fig. 9. The $|\text{AF4}\rangle$ ground state breaks translational symmetry such that blocks with different signs alternate. Hence, the upper (lower) sign should be taken for an even (odd) cell of the $|\text{AF4}\rangle$ state.

Case	Heisenberg-Ising				Heisenberg		
	Ground-state label	$S_{i,1}^z$	σ_i	$S_{i,2}^z + S_{i,3}^z$	$S_{i,1}^z$	$S_{i,4}^z$	$T_i^z = S_{i,2}^z + S_{i,3}^z$
Figs. 9(a),(b), $M = 0$	AF2	-0.4621	1/2	0.9621	-	-	-
Fig. 9(c), $M = 0$	AF4	$\mp 1/6$	$\pm 1/2$	$\pm 2/3$	-	-	-
Fig. 9(a), $M = 1/2$	F3	-1/6	1/2	2/3	0.2640	0.2640	0.4720 ⁶³
Fig. 9(b), $M = 1/2$	F2	1/2	1/2	0	1/2	1/2	0
Fig. 9(c), $M = 1/2$	F4	1/6	1/2	1/3	-0.0799	0.4287	0.6512 ⁶³

particular, we conclude that the $M = 1/2$ plateau survives for $N = \infty$. All further plateaux in the magnetization curve of the Heisenberg model are probably gone.

3. $K_1 < 0$

Fig. 9 shows three examples of magnetization curves with ferromagnetic $K_1 < 0$ and potentially a further ferromagnetic exchange constant. In all three cases shown in Fig. 9, the Heisenberg-Ising model has plateaux at $M = 0$ and $1/2$, separated by jumps in the magnetization curve. These two plateaux are also present in the Heisenberg model. However, in the case $J_1 = J = 1$ and $K_1 = K_2 = -1$ a finite-size analysis is again necessary to show that the spin gap (corresponding to the $M = 0$ plateau) persists in the thermodynamic limit. According to the data shown in the inset of Fig. 9(c), we expect $N = 96$ to be a good approximation to the thermodynamic limit even if the spin gap decreases substantially with growing N for the smallest values of N considered.

At a quantitative level, the spin gap of the Heisenberg model compares favorably to that of the Heisenberg-Ising model in the case of Fig. 9(a) and the width of the $M = 1/2$ plateau compares favorably in all three cases presented in Fig. 9. The best agreement is observed for the case presented in Fig. 9(b) ($J_1 = J = 1$, $K_1 = K_2 = -1$). In this case, the jump between $M = 1/2$ and 1 is reproduced exactly and both models give rise to a jump at the lower edge of the $M = 1/2$ plateau, albeit not exactly at the same magnetic field.

For the three examples shown in Fig. 9, the spin gap of the Heisenberg model always arises out of a periodic pattern $T_i = 1$. This conclusion agrees with Ref. 44 in the case of Figs. 9(a) and (b). In fact, the behavior at low magnetic fields is identical in these two cases, including the feature at low magnetizations in Fig. 9(b). To the best of our knowledge, the case presented in Fig. 9(c) has not been discussed previously. The ground state of the Heisenberg-Ising system at $M = 0$ is the $|\text{AF2}\rangle$ one in the case of Figs. 9(a) and (b) and the $|\text{AF4}\rangle$ one in the case of Fig. 9(c). The corresponding local spin expectation values are given in Table X. In the Heisenberg model at zero magnetization, individual spin expectation values vanish for symmetry reasons. Hence, for the Heisenberg

model at $M = 0$, we have to look at correlation functions in order to determine the structure of the ground state. Fig. 10 shows selected correlation functions computed by exact diagonalization for a periodic $N = 32$ system as a function of distance j between cells. The correlations of the left panel reveal a structure which is similar to the $|\text{AF2}\rangle$ state, *i.e.*, the spins $S_{i,1}^z$ and $S_{i,4}^z$ next to the composite spin T_i^z point in the opposite direction of this composite spin while spins of the same type show a tendency of aligning parallel between different cells. By contrast, in the right panel of Fig. 10 one observes a tendency of *antiparallel* alignment between cells at an odd distance while the internal structure of a cell is the same as before, as expected for the $|\text{AF4}\rangle$ state. In the case of the left panel of Fig. 10, correlations are short-ranged while for the right panel they decay more slowly in accordance with the size of the spin gap (given by the width of the $M = 0$ plateau) in Figs. 9(a),(b) and Fig. 9(c), respectively. Overall, we conclude that for all three cases considered in Fig. 9, the $M = 0$ ground state of the Heisenberg-Ising model is a good qualitative representation of the $M = 0$ ground state of the Heisenberg model.

Turning to finite magnetizations, we observe that in the case of Figs. 9(a) and (c), the $M = 1/2$ plateau state of the Heisenberg model arises out of a system with all $T_i = 1$ while in the case of Fig. 9(b) it is characterized by all $T_i = 0$. The corresponding local spin expectation values are given in Table X. The ground states of the Heisenberg-Ising model corresponding to the $M = 1/2$ plateau in the three cases presented in Figs. 9(a), (b), and (c) are $|\text{F3}\rangle$, $|\text{F2}\rangle$, and $|\text{F4}\rangle$, respectively. The spin expectation values for these states are included in Table X. Note that the $|\text{F4}\rangle$ state is macroscopically degenerate (see Eq. (20)) such that the average over this manifold yields effectively the average of the local expectation values in the $|\text{F2}\rangle$ and $|\text{F3}\rangle$ states. In the case of Fig. 9(a), the reflection-symmetry breaking interactions of the Heisenberg-Ising model lead to a breaking of reflection symmetry in the $M = 1/2$ state which is not present in the Heisenberg model. Otherwise, the structure of the $M = 1/2$ states of the Heisenberg-Ising and Heisenberg model is at least similar in the case of Figs. 9(a) and (c). In the case of Fig. 9(b) we even find an identical $M = 1/2$ state as reflected by identical local spin expectation val-

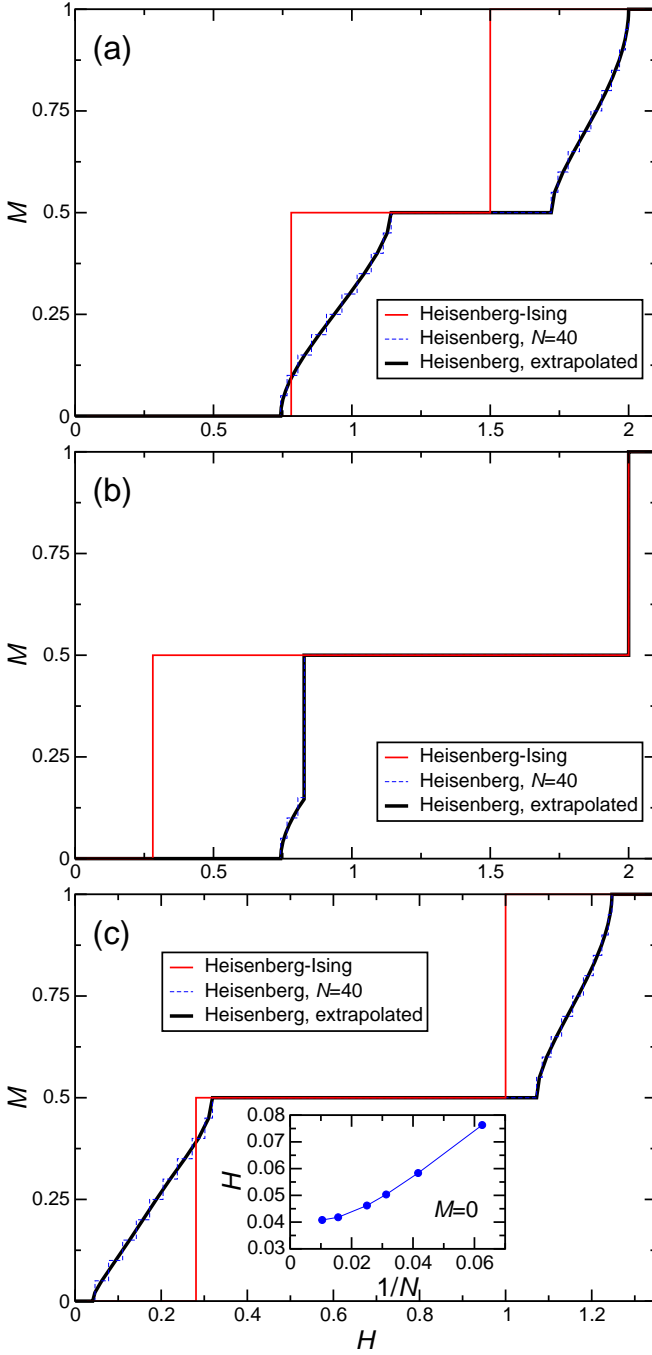


FIG. 9. (Color online) Same as Fig. 8, but for cases which contain ferromagnetic exchange constants, namely $J_1 = K_1 = -1$, $J = K_2 = 1$ (a), $J_1 = J = K_2 = 1$, $K_1 = -1$ (b), and $J_1 = J = 1$, $K_1 = K_2 = -1$ (c). The inset of panel (c) shows the finite-size behavior of the spin gap (edge of the $M = 0$ plateau) at $J_1 = J = 1$, $K_1 = K_2 = -1$.

ues for the Heisenberg-Ising and Heisenberg model.

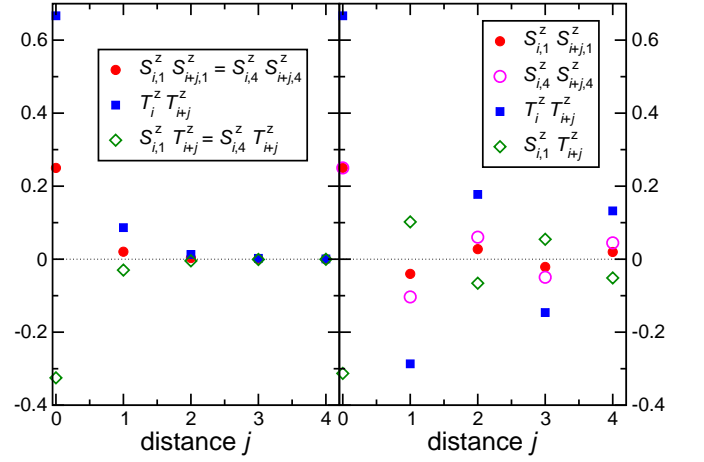


FIG. 10. (Color online) Correlation functions of the z -components for the Heisenberg model with $N = 32$ sites at $M = 0$. j measures the distance in units of cells; due to the periodic boundary conditions, the maximum accessible distance is $N/8 = 4$. The left panel is for $J_1 = \pm 1$, $J = K_2 = 1$, $K_1 = -1$ whereas the right panel shows results for $J_1 = J = 1$, $K_1 = K_2 = -1$.

C. Entropy and cooling rate

We now turn to thermodynamic properties. Since one of the most important properties of the present type of models is the magnetocaloric effect,^{13,46–49,55,64–68} we focus on the entropy S as a function of magnetic field H and temperature T as well as the adiabatic cooling rate as a function of magnetic field. These quantities have been computed for the Heisenberg model by full diagonalization.

The orthogonal arrangement of dimers in our model is very similar to the two-dimensional Shastry-Sutherland model.⁶⁹ The latter model is found to have a good realization in $\text{SrCu}_2(\text{BO}_3)_2$ with a ratio between dimer and plaquette couplings estimated to be close to 0.7 (see Ref. 70 for a review). Hence, the case $J_1 = K_1 = 1$, $J = K_2 = 0.7$ can be viewed as the one-dimensional counterpart of the two-dimensional Shastry-Sutherland model for $\text{SrCu}_2(\text{BO}_3)_2$. Indeed, in this parameter regime, both the one- and two-dimensional Heisenberg model have an exact dimer ground state (compare section VIB and Ref. 69, respectively) and it was noted early on that the magnetization curve of $\text{SrCu}_2(\text{BO}_3)_2$ increases very steeply above a magnetic field $H \approx 20\text{T}$, like a system of isolated dimers⁷¹ or the one-dimensional model, see Fig. 8(a).

Fig. 11 shows our results for the entropy per spin S/N at $J_1 = K_1 = 1$, $J = K_2 = 0.7$ as a function of magnetic field H and temperature T . Here we focus on magnetic fields corresponding to magnetizations $M \leq 1/4$. At a quantitative level there are certain differences between the Heisenberg-Ising model (top panel of Fig. 11) and the Heisenberg model (bottom panel).

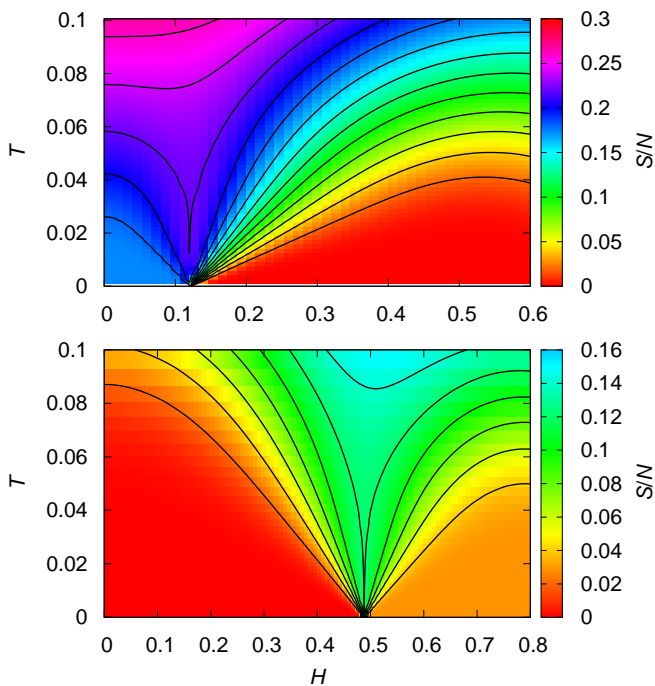


FIG. 11. (Color online) Entropy per spin S/N as a function of H and T for $J_1 = K_1 = 1, J = K_2 = 0.7$. The top panel shows results for the Heisenberg-Ising model in the thermodynamic limit and the lower panel the Heisenberg model with $N = 24$ spins. Lines show values of constant entropy, starting with $S/N = 0.02$ at the bottom and increasing in steps of 0.02.

Firstly, from the magnetization curve Fig. 8(a) we already know that the transition field H_c between the $M = 0$ and $1/4$ states is shifted. Secondly, we also know that the $M = 0$ state of the Heisenberg model is non-degenerate whereas the Heisenberg-Ising model has a macroscopic degeneracy giving rise to a residual entropy $S/N = \ln 2/4 = 0.173\dots$, and accordingly, the values of S differ in the low-field low-temperature regime of Fig. 11. Nevertheless, the Heisenberg-Ising model and the Heisenberg model share important qualitative features. In particular, in both cases another local excitation comes down as $H \rightarrow H_c$. Noting that in the *Heisenberg model* these local excitations are not allowed to occupy two consecutive blocks for $M \leq 1/2$, one can count the degeneracy at $H = H_c$ using a 2×2 transfer matrix^{1,32,64} and finds $S/N = \ln((1 + \sqrt{5})/2)/4 = 0.120\dots$ in the limit $T \rightarrow 0$. A similar 3×3 transfer-matrix procedure for the *Heisenberg-Ising model* yields $S/N = \ln(1 + \sqrt{2})/4 = 0.220\dots = \ln 2/4 + 0.047\dots$ for the zero-temperature limit at $H = H_c$. Recall also that the ground state at $M = 1/4$ is two-fold degenerate. For the $N = 24$ system shown in the lower panel of Fig. 11, this gives rise to a finite-size value $S/N = \ln 2/24 = 0.028\dots$ for $H > H_c$ and in the limit $T \rightarrow 0$.

The additional residual entropy at $H = H_c$ gives rise to

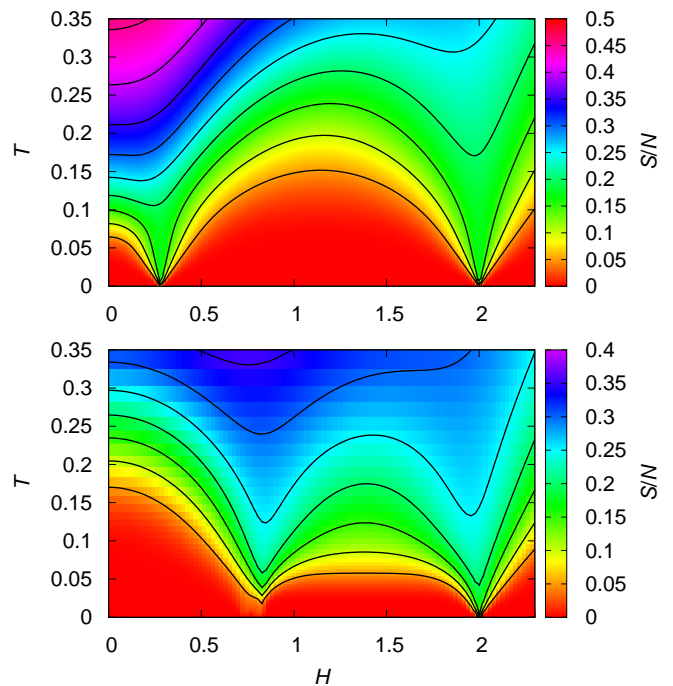


FIG. 12. (Color online) Entropy per spin S/N as a function of H and T for $J_1 = J = K_2 = 1, K_1 = -1$. The top panel shows results for the Heisenberg-Ising model in the thermodynamic limit and the lower panel the Heisenberg model with $N = 24$ spins. Lines show values of constant entropy, starting with $S/N = 0.05$ at the bottom and increasing in steps of 0.05.

substantial cooling during adiabatic (de)magnetization, as also demonstrated by the constant entropy curves in Fig. 11. In fact, if one starts with a sufficiently low temperature at $H = 0$, one reaches $T = 0$ as H approaches H_c , both in the Heisenberg model and the Heisenberg-Ising model. Similar behavior is suggested in the two-dimensional Shastry-Sutherland model by the flat triplet branch above the dimerized ground state.⁷² Indeed, there is indirect evidence for substantial cooling in $\text{SrCu}_2(\text{BO}_3)_2$ during pulse-field magnetization experiments.⁷³

The other case of special interest is $J_1 = J = K_2 = 1, K_1 = -1$. Not only does Fig. 9(b) demonstrate quantitative agreement between the Heisenberg model and the Heisenberg-Ising model at the saturation field, but this case can also be considered as a realization of the hard-monomer universality class of localized magnons.^{46–49}

Fig. 12 shows the entropy per site S/N for the Heisenberg-Ising model (top panel) and the Heisenberg model (lower panel) at $J_1 = J = K_2 = 1, K_1 = -1$. The global behavior of both models is similar. The main qualitative difference can be observed at small magnetic fields when the zero-field gap is closing: the Heisenberg-Ising model has a macroscopic ground-state degeneracy $S/N = \ln 2/4$ at the position of the first step in the magnetization curve Fig. 9(b) whereas in the Heisenberg

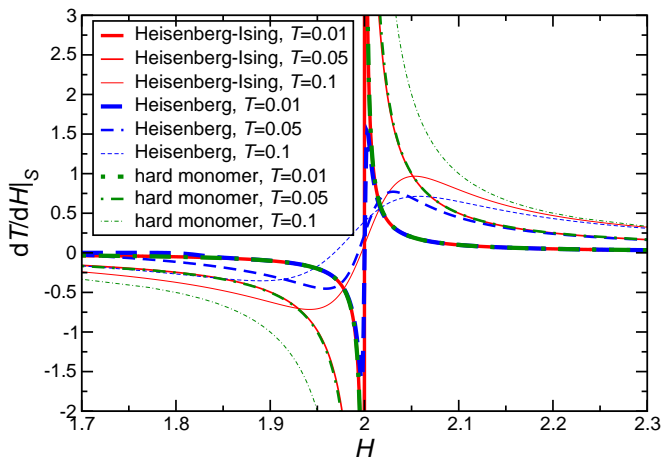


FIG. 13. (Color online) Adiabatic cooling rate as a function of magnetic field H for three different temperatures at $J_1 = J = K_2 = 1$, $K_1 = -1$. Results for the Heisenberg-Ising model and hard monomers are for the thermodynamic limit while those for the Heisenberg model are for $N = 24$ spins.

model the degeneracy is lifted in correspondence with the smoother transition. Nevertheless, also the Heisenberg model exhibits an enhanced low-temperature entropy as the $T = 0$ magnetization increases from $M = 0$ to $1/2$. This enhanced entropy is reflected by the minimum in the constant entropy curves in the lower panel of Fig. 12.

Close to the saturation field $H = 2$ we find even quantitative agreement between the Heisenberg-Ising and Heisenberg model. In particular, both models now give rise to a zero-temperature entropy $S/N = \ln 2/4$ at $H = 2$ such that one could cool to arbitrarily low temperatures by adiabatic magnetization or demagnetization when approaching the saturation field from below or above, respectively. Note that in this regime finite-size effects are very small, as is evident, e.g., from the effective hard-monomer description.^{46–49} Hence, we can use our $N = 24$ exact diagonalization data for reference.

For a more detailed comparison we use the adiabatic cooling rate which can be written as

$$\left. \frac{dT}{dH} \right|_S = - \frac{\partial S / \partial H|_T}{\partial S / \partial T|_H}. \quad (28)$$

This is nothing else but the slope of the constant entropy curves in Figs. 11 and 12. The adiabatic cooling rate has the advantage over the entropy that it is directly accessible in experiments.^{74–76}

For hard monomers, the right-hand side of Eq. (28) can be evaluated easily using the free energy per unit cell $f = -T \ln(1 + \exp(-(H - H_c)/T))$ and $S = -\partial f / \partial T$:

$$\left. \frac{dT}{dH} \right|_S^{\text{monomer}} = \frac{T}{H - H_c}. \quad (29)$$

Fig. 13 compares the cooling rate for the Heisenberg model, the Heisenberg-Ising model, and the effective hard

monomer low-energy description for the same parameters as in Fig. 12 for three different temperatures. All three descriptions exhibit a strongly enhanced cooling rate for $H \approx H_c = 2$ which reflects the $T = 0$ entropy at $H_c = 2$ (see Fig. 12). Not surprisingly, the quantitative agreement between the different descriptions is best at the lowest temperature $T = 0.01$. The main difference between the Heisenberg-Ising model and hard monomers is that the singularity in Eq. (29) at $H = H_c$ and any $T > 0$ is removed in the Heisenberg-Ising model by the presence of further degrees of freedom at higher energies. This improves the agreement with the full Heisenberg model at higher temperatures.

VII. CONCLUSION

We have presented a detailed analysis of the ground states and magnetic properties of a one-dimensional lattice spin model with a structure which is very similar to the famous orthogonal dimer chain,^{28–31} although the exchange constants are more general. In the Heisenberg-Ising variant, the main ingredient is the block structure of the Hamiltonian. Each block consists of a triangle of $s = 1/2$ spins interacting with each other via an XXZ -interaction and of one single spin, which is connected to two “dimer” spins from the triangle by Ising bonds. This particular structure renders the system exactly solvable by the classical transfer-matrix method.

First, we investigated the large variety of $T = 0$ ground states in an external magnetic field. Some of the ground states break translational symmetry spontaneously, thus giving rise to doubling of the unit cell. Moreover, we found two macroscopically degenerate ground states. One of them, the zero-magnetization state $|AF1\rangle$, is the closest analog of the famous dimerized ground state of the underlying purely quantum orthogonal dimer chain.^{28–30} The main difference is that the Heisenberg-Ising system cannot form a quantum dimer on the horizontal bond, but instead the two classical antiparallel spin configurations are equally likely to be found on each given horizontal bond, thus yielding a two-fold degeneracy per block. The other ground state with a two-fold degeneracy per block, $|F4\rangle$, carries magnetization $M = 1/2$ and has a different origin. It appears only at very symmetric values of parameters and corresponds to a degeneracy between the symmetric and antisymmetric $S_{\text{tot}}^z = 1/2$ ground states for the two coupled quantum spins on a vertical dimer.

The second focus of our investigation was a comparison of the Heisenberg-Ising model with numerical results for the full Heisenberg model. Certain features of the full Heisenberg model are not present in the Heisenberg-Ising variant. For example, for certain antiferromagnetic values of the exchange constants, the Heisenberg model also exhibits ground states with a periodicity larger than two,^{30,44} and relatedly an infinite sequence of plateaux in its magnetization curve.³⁰ Only the main plateaux at $M = 0, 1/2$, and $1/4$ are also present in the Heisenberg-

Ising variant.

When considered as an approximation to the Heisenberg model, the Heisenberg-Ising model performs in general better if some of the Ising exchanges are ferromagnetic. In the three examples with a ferromagnetic $K_1 < 0$ which we have discussed, the presence and nature of plateaux at $M = 0$ and $1/2$ is qualitatively reproduced to the extent possible. Between these plateaux, the Heisenberg-Ising model always yields jumps in the $T = 0$ magnetization curve while the Heisenberg model may exhibit smooth transitions. Also the critical fields can differ noticeably. Remarkably, in the case $J_1 = J = K_2 = 1$, $K_1 = -1$ we found that the Heisenberg-Ising model reproduces results for the Heisenberg model even at a quantitative level close to the saturation field (see Figs. 9(b) and 13). This exact correspondence may be attributed to the product-state structure of the low-energy states of the Heisenberg model in this parameter regime,⁴⁶⁻⁴⁹ and we speculate that it is generic for a sufficiently strong coupling of the vertical dimer exchange J_1 .

We believe that further continuation of recent developments in the field of magnetochemistry²²⁻²⁷ will make it possible to obtain magnetic materials which match the model considered in the present paper. At the mo-

ment, the most direct application of our system probably is as a one-dimensional version of the two-dimensional Shastry-Sutherland model for $\text{SrCu}_2(\text{BO}_3)_2$.⁷⁰ In particular, we have observed an enhanced magnetocaloric effect upon closing the zero-field spin gap, both in the one-dimensional Heisenberg as well as its simplified Heisenberg-Ising variant, in accordance with indirect evidence for cooling by adiabatic magnetization of $\text{SrCu}_2(\text{BO}_3)_2$.⁷³

ACKNOWLEDGMENTS

V.O. expresses his gratitude to the Institut für Theoretische Physik of Göttingen University for the warm hospitality during the course of this project. This work was supported by the DFG (projects No. HO 2325/4-2, HO 2325/5-1, HO 2325/7-1, and HO 2325/8-1). V.O. also acknowledges support from a joint grant of CRDF-NFSAT and the State Committee of Science of Republic of Armenia ECSP-09-94-SASP,SCS-BFBR 11RB-001, Volkswagen Foundation (grant No. I/84 496), and ANSEF-2497-PS.

* ohanyan@yerphi.am

¹ R. Baxter, *Exactly Solved Models in Statistical Mechanics*, (Academic Press, New York, 1982).
² M. Takahashi, *Thermodynamics of One-dimensional Solvable Models*, (Cambridge: Cambridge University Press, 1999).
³ H. Bethe, *Z. Physik* **71**, 205 (1931).
⁴ A. P. Isaev, *Phys. Particles Nuclei* **26**, 501 (1995).
⁵ C. Gómez, M. Ruiz-Altaba, and G. Sierra, *Quantum Groups in Two-Dimensional Physics*, (Cambridge: Cambridge University Press, 2005).
⁶ A. Klümper, *Lect. Notes Phys.* **645**, 349 (2004); A. Klümper, *Eur. Phys. J. B* **5**, 677 (1998); C. Trippé, A. Honecker, A. Klümper, and V. Ohanyan, *Phys. Rev. B* **81**, 054402 (2010).
⁷ N. S. Ananikyan, Sh. A. Hairyan, E. Sh. Mamasahlisov, and V. F. Morozov, *Biopolymers* **30**, 357 (1990); N. Ananikian, L. Ananikyan, and R. Artuso, *Phys. Lett. A* **360**, 615 (2007); N. Ananikian, L. Ananikyan, R. Artuso, and K. Sargsyan, *Physica A* **387**, 5433 (2008); A. V. Badasyan, A. Giacometti, Y. Sh. Mamasahlisov, V. F. Morozov, and A. S. Benight, *Phys. Rev. E* **81**, 021921 (2010).
⁸ S. T. Dembiński and T. Wydro, *phys. stat. sol. (b)* **67**, K123 (1975).
⁹ V. Ohanyan and N. Ananikian, *Phys. Lett. A* **307**, 76 (2003).
¹⁰ E. Aydiner and C. Akyüz, *Chin. Phys. Lett.* **22**, 2382 (2005); E. Aydiner, C. Akyüz, M. Gönülol, and H. Polat, *phys. stat. sol.(b)* **243**, 2901 (2006).
¹¹ J. Strečka, M. Hagiwara, M. Jaščur, and K. Minami, *Czech. J. Phys.* **54**, D583 (2004); J. Strečka, M. Jaščur, M. Hagiwara, K. Minami, Y. Narumi, and K. Kindo, *Phys.*

Rev. B **72**, 024459 (2005).
¹² J. Strečka and M. Jaščur, *J. Phys.: Condens. Matter* **15**, 4519 (2003); J. Strečka, L. Čanová, T. Lučivjanský, and M. Jaščur, *J. Phys.: Conf. Ser.* **145**, 012058 (2009).
¹³ L. Čanová, J. Strečka, and M. Jaščur, *J. Phys.: Condens. Matter* **18**, 4967 (2006); L. Čanová, J. Strečka, and T. Lučivjanský, *Condensed Matter Physics* **12**, 353 (2009).
¹⁴ J. S. Valverde, O. Rojas, and S. M. de Souza, *J. Phys.: Condens. Matter* **20**, 345208 (2008).
¹⁵ D. Antonosyan, S. Bellucci, and V. Ohanyan, *Phys. Rev. B* **79**, 014432 (2009); V. Ohanyan, *Phys. Atom. Nucl.* **73**, 494 (2010).
¹⁶ V. Ohanyan, *Condensed Matter Physics* **12**, 343 (2009).
¹⁷ S. Bellucci and V. Ohanyan, *Eur. Phys. J. B* **75**, 531 (2010).
¹⁸ O. Rojas, S. M. de Souza, V. Ohanyan, and M. Khurshudyan, *Phys. Rev. B* **83**, 094430 (2011).
¹⁹ L. Chakhmakhchyan, N. Ananikian, L. Ananikyan, and Č. Burdík, *J. Phys.: Conf. Ser.* **343**, 012022 (2012).
²⁰ M. S. S. Pereira, F. A. B. F. de Moura, and M. L. Lyra, *Phys. Rev. B* **77**, 024402 (2008); M. S. S. Pereira, F. A. B. F. de Moura, and M. L. Lyra, *Phys. Rev. B* **79**, 054427 (2009).
²¹ B. M. Lisnii, *Low Temp. Phys.* **37**, 296 (2011).
²² D. Visinescu, A. M. Madalan, M. Andruh, C. Duhayon, J.-P. Sutter, L. Ungur, W. Van den Heuvel, and L. F. Chibotaru, *Chem. Eur. J.* **15**, 11808 (2009).
²³ J. Rinck, G. Novitchi, W. Van den Heuvel, L. Ungur, Y. Lan, W. Wernsdorfer, C. E. Anson, L. F. Chibotaru, and A. K. Powell, *Angew. Chem., Int. Ed.* **49**, 7583 (2010).
²⁴ W. Van den Heuvel and L. F. Chibotaru, *Phys. Rev. B* **82**, 174436 (2010).

- ²⁵ V. Ravi Chandra, S. Ramasesha, and D. Sen, Phys. Rev. B **70**, 144404 (2004).
- ²⁶ T. S. Venkatakrisnan, S. Sahoo, Nicolas Bréfuel, C. Duhayon, C. Paulsen, A.-L. Barra, S. Ramasesha, and J.-P. Sutter, J. Am. Chem. Soc. **132**, 6047 (2010).
- ²⁷ S. Sahoo, J.-P. Sutter, and S. Ramasesha, J. Stat. Phys. **147**, 181 (2012).
- ²⁸ J. Richter, N. B. Ivanov, and J. Schulenburg, J. Phys.: Condens. Matter **10**, 3635 (1998).
- ²⁹ A. Koga, K. Okunishi, and N. Kawakami, Phys. Rev. B **62**, 5558 (2000).
- ³⁰ J. Schulenburg and J. Richter, Phys. Rev. B **65**, 054420 (2002).
- ³¹ A. Honecker, J. Schulenburg, and J. Richter, J. Phys.: Condens. Matter **16**, S749 (2004).
- ³² K. Huang, *Statistical Mechanics*, (John Wiley & Sons, New York, 1963).
- ³³ Here and below we set $H_1 = H_2 \equiv H$.
- ³⁴ M. Oshikawa, M. Yamanaka, and I. Affleck, Phys. Rev. Lett. **78**, 1984 (1997).
- ³⁵ M. P. Gelfand, Phys. Rev. B **43**, 8644 (1991).
- ³⁶ K. Takano, K. Kubo, and H. Sakamoto, J. Phys.: Condens. Matter **8**, 6405 (1996).
- ³⁷ N. B. Ivanov and J. Richter, Phys. Lett. A **232**, 308 (1997).
- ³⁸ M. Mambri, J. Trébos, and F. Mila, Phys. Rev. B **59**, 13806 (1999).
- ³⁹ A. Honecker, F. Mila, and M. Troyer, Eur. Phys. J. B **15**, 227 (2000).
- ⁴⁰ C. Gros, R. Valentí, J. V. Alvarez, K. Hamacher, and W. Wenzel, Phys. Rev. B **62**, R14617 (2000).
- ⁴¹ S. Trebst and A. Sengupta, Phys. Rev. B **62**, R14613 (2000).
- ⁴² A. Honecker and W. Brenig, Phys. Rev. B **63**, 144416 (2001).
- ⁴³ E. Chattopadhyay and I. Bose, Phys. Rev. B **65**, 134425 (2002).
- ⁴⁴ J. Schulenburg and J. Richter, Phys. Rev. B **66**, 134419 (2002).
- ⁴⁵ O. Rojas and F. C. Alcaraz, Phys. Rev. B **67**, 174401 (2003).
- ⁴⁶ O. Derzhko and J. Richter, Phys. Rev. B **70**, 104415 (2004).
- ⁴⁷ J. Richter, Low Temp. Phys. **31**, 695 (2005).
- ⁴⁸ O. Derzhko and J. Richter, Eur. Phys. J. B **52**, 23 (2006).
- ⁴⁹ O. Derzhko, J. Richter, A. Honecker, and H.-J. Schmidt, Low Temp. Phys. **33**, 745 (2007).
- ⁵⁰ N. B. Ivanov, J. Richter, and J. Schulenburg, Phys. Rev. B **79**, 104412 (2009).
- ⁵¹ O. Derzhko, T. Krokhmalkii, and J. Richter, Phys. Rev. B **82**, 214412 (2010).
- ⁵² K. Hida, K. Takano, and H. Suzuki, J. Phys. Soc. Jpn. **79**, 044702 (2010).
- ⁵³ K. Hida, K. Takano, and H. Suzuki, J. Phys. Soc. Jpn. **79**, 114703 (2010).
- ⁵⁴ S. R. Manmana, J.-P. Picon, K. P. Schmidt, and F. Mila, Europhys. Lett. **94**, 67004 (2011).
- ⁵⁵ A. Honecker, S. Hu, R. Peters, and J. Richter, J. Phys.: Condens. Matter **23**, 164211 (2011).
- ⁵⁶ M. Maksymenko, O. Derzhko, and J. Richter, Eur. Phys. J. B **84**, 397 (2011).
- ⁵⁷ K. Hida and K. Takano, J. Phys. Soc. Jpn. **80**, 104710 (2011).
- ⁵⁸ J. C. Bonner and M. E. Fisher, Phys. Rev. **135**, A640 (1964).
- ⁵⁹ J. B. Parkinson and J. C. Bonner, Phys. Rev. B **32**, 4703 (1985).
- ⁶⁰ A. F. Albuquerque, F. Alet, P. Corboz, P. Dayal, A. Feiguin, S. Fuchs, L. Gamper, E. Gull, S. Gürtler, A. Honecker, R. Igarashi, M. Körner, A. Kozhevnikov, A. Läuchli, S. R. Manmana, M. Matsumoto, I. P. McCulloch, F. Michel, R. M. Noack, G. Pawłowski, L. Pollet, T. Pruschke, U. Schollwöck, S. Todo, S. Trebst, M. Troyer, P. Werner, and S. Wessel, J. Magn. Magn. Mater. **310**, 1187 (2007).
- ⁶¹ S. R. White, Phys. Rev. Lett. **69**, 2863 (1992).
- ⁶² U. Schollwöck, Rev. Mod. Phys. **77**, 259 (2005).
- ⁶³ The numbers quoted are actually for an $N = 96$ periodic system. However, comparison with smaller system sizes demonstrates that all given digits can be considered representative of the thermodynamic limit $N = \infty$.
- ⁶⁴ M. E. Zhitomirsky and A. Honecker, J. Stat. Mech.: Theor. Exp. P07012 (2004).
- ⁶⁵ M. E. Zhitomirsky and H. Tsunetsugu, Phys. Rev. B **70**, 100403(R) (2004).
- ⁶⁶ M. E. Zhitomirsky and H. Tsunetsugu, Prog. Theor. Phys. Suppl. **160**, 36 (2005).
- ⁶⁷ J. Schnack, H.-J. Schmidt, A. Honecker, J. Schulenburg, and J. Richter, J. Phys.: Conf. Ser. **51**, 43 (2006).
- ⁶⁸ J. Richter, O. Derzhko, and A. Honecker, Int. Jour. Mod. Phys. B **22**, 4418 (2008).
- ⁶⁹ B. S. Shastry and B. Sutherland, Physica **108B**, 1069 (1981).
- ⁷⁰ S. Miyahara and K. Ueda, J. Phys.: Condens. Matter **15**, R327 (2003).
- ⁷¹ H. Kageyama, K. Yoshimura, R. Stern, N. V. Mushnikov, K. Onizuka, M. Kato, K. Kosuge, C. P. Slichter, T. Goto, and Y. Ueda, Phys. Rev. Lett. **82**, 3168 (1999).
- ⁷² Zheng Weihong, C. J. Hamer, and J. Oitmaa, Phys. Rev. B **60**, 6608 (1999).
- ⁷³ F. Levy, I. Sheikin, C. Berthier, M. Horvatić, M. Takigawa, H. Kageyama, T. Waki, and Y. Ueda, Europhys. Lett. **81**, 67004 (2008).
- ⁷⁴ M. Lang, Y. Tsui, B. Wolf, D. Jaiswal-Nagar, U. Tutsch, A. Honecker, K. Remović-Langer, A. Prokofiev, W. Assmus, and G. Donath, J. Low Temp. Phys. **159**, 88 (2010).
- ⁷⁵ Y. Tokiwa and P. Gegenwart, Rev. Sci. Instrum. **82**, 013905 (2011).
- ⁷⁶ B. Wolf, Y. Tsui, D. Jaiswal-Nagar, U. Tutsch, A. Honecker, K. Remović-Langer, G. Hofmann, A. Prokofiev, W. Assmus, G. Donath, and M. Lang, PNAS **108**, 6862 (2011).